On the dynamics of relativistic multi-layer spherical shell systems

Merse E. Gáspár and István Rácz

RMKI, H-1121 Budapest, Konkoly Thege Miklós út 29-33. Hungary

E-mail: merse@rmki.kfki.hu, iracz@rmki.kfki.hu

Abstract. The relativistic time evolution of multi-layer spherically symmetric shell systems—consisting infinitely thin shells separated by vacuum regions—is examined. **Besides providing a brief review of the basics of the formalism, in particular, the equations of motion and the criteria singling out the allowed initial conditions are also discussed.** Whenever two shells collide the evolution is continued with the assumption that the collision is **either** totally transparent **or totally inelastic**. The time evolution of various multi-layer shell systems—comprised by large number of shells **mimicing thereby the behavior of a thick shell making it possible to study the formation of acoustic singularity**—is analyzed numerically and compared in certain cases to the corresponding Newtonian time evolution. The analytic setup is chosen such that the developed code is capable to follow the evolution even inside the black hole region. This, in particular, allowed us to investigate the mass inflation phenomenon in the **chosen** framework **of multi-layer spherically symmetric shell systems**.

PACS numbers: 04.20.-q, 04.25.-g

1. Introduction

Relativistic infinitely thin spherical shells plays important role in various dynamical contexts ranging from microscopic to astrophysical systems. **In the following, without trying to have a complete list, we intend to line up some of the most characteristic ones. To start off recall that For instance,** by applying a charged shell as an electron model one may avoid the appearance of negative gravitational mass caused by the concentration of charge at the center [1, 2, 3]. Using families of spherically symmetric thin shells instead of spherically symmetric continuous matter distributions reduces significantly the complexity of evolutionary problems as the dynamics of thin shells may be investigated by using various analogies from the description of the motion of a particle in a one-dimensional effective potential. **Due to this setup even Accordingly,** the quantization of systems **built up from comprised by** thin shells **gets to be simplified significantly is tractable** [2, 4, 5]. Macroscopically stable quark-gluon matter can also be studied with a toy model in which relativistic shells and the MIT bag model are combined together [6]. Collapsing dust shells can be use to probe

stability or studying energetics of compact objects such as back holes or star models mimicing the properties of black holes [7, 8]. Shells can be used **in simplifying the to** model **of** matter ejection at certain phases of supernova explosions [9] or in modeling supernova remnants [10]. More realistic radiating shell models can also be constructed [11] and with the help of these models, even the critical collapse may analytically be investigated [12]. With the help of infinitesimally thin shells one can construct exact solutions by gluing together spherically symmetric spacetime domains. This way exotic models such as gravastars [13, 14] or wormholes [15, 16, 17, 18, 19, 20] may also be **created studied**. Simple models of large scale voids in galaxy distributions can also be constructed with the help of shells [21, 22, 23]. Dynamics of spherical shells comes to play in some cosmological models, such as higher dimensional brane cosmologies, in which it is assumed that our four-dimensional Universe is merely a surface living in a higher dimensional spacetime [24]. Shells do play central role in the bubble inflation model of the early universe [25, 26, 27, 28, 29]. It is widely held that by studying dynamics of shells important phenomena such as the focusing singularity at the center [30] or the so called acoustic singularity—this will be discussed later on Section 4.1.—can also be studied.

The basic equations governing the dynamics of thin shells can be derived in various ways. For instance, by making use of the junction conditions of the metrics [31, 32, 33, 35, 36, 37, 38], by applying distributions [39, 40, 41] or the variational Jacobi–Hamiltonian approach [42, 43, 44, 45, 46], or by deriving them **as by taking** a limit of **that of the evolution equations of** the thick shells [47, 48]. It is important to mention that all of these methods end up with the same set of basic equations.

In describing the evolution of families of infinitesimally thin shells the study of their crossing is essential. Nevertheless much less have been done in this respect. For instance, the basic equations describing shell crossing have been derived only for some specific cases, such as the totally transparent [49, 36, 50] or the totally inelastic collisions [51, 8]. Nevertheless, most of the authors do not go beyond deriving the equations of motion for dust shells, or studying only the simplest possible analytic cases. This, in particular, means that almost no result is available for multi-layer shell systems with generic equation of state (EOS). Concerning what has been done, apparently, there are only two papers in the literature which carries out **the a** systematic study of the dynamics of more than two shells or consider the evolution of shell systems such that **'multiple' collisions of the shells shell crossings** are allowed. In [49] the dynamics of star clusters is studied, although considerations therein remain on the theoretical side providing only the generic equations of motion in Schwarzschild time coordinates which, in particular, does not allow the study of the motion through the event horizon. In [50] the dynamics of two dust shells**, with zero central mass,** was investigated with the use of Kruskal–**Szekeres** coordinates**, due to which—thereby** the authors were able to follow the motion of the system below the horizon**, —**and **when collisions happened they were restrected shell crossings were assumed** to be **totally** transparent.

Our main aim in this paper is to present some new results concerning the dynamics of multi-layer shell systems with **allowing the occurrence of collisions during the evolution the inclusion of of shell crossings**. **In carrying out t** The corresponding dynamical investigations **we have developed an effective were done by using of a** C++ code which made the study of evolution of systems composed by a large number of shells and with generic EOS to be possible [52]. In Section 2 some of the basics related to the analytic description of the motion of a single shell are recalled using Schwarzschild and ingoing Eddington–Finkelstein 'time' coordinates. For comparison, the corresponding Newtonian case is also discussed. **In addition, some delicate issues related to the choice of initial conditions are reviewed and the basic properties of the dynamics for linear EOSs are summarized.** In Section 3, for the sake of simplicity, first only the interaction of two shells is considered providing the ballance equations for the case totally transparent **and totally inelastic collisions shell crossings**. In Section 4, the time evolution of systems comprised by a large number of concentric shells—in particular, the formation of acoustic singularities—is investigated. One of the main advantage of the method applied in this paper is related to the use of ingoing Eddington–Finkelstein coordinates which allows us to evolve even very comlex composite systems throughout the entire spacetime including the black hole region. As one of the most important outcome of the corresponding investigations is that the phenomena of mass inflation could also be studied by making use of colliding thin shells. The paper is closed by our final remarks.

Throughout this paper, the geometrized units are used, with $G = c = 1$, and the abstract index notation of [53] will be applied with the additional use of uppercase Latin indices signifying quantities living on three-dimensional hypersurfaces.

2. The dynamics of a single shell

In this section the basic equations relevant for a spherically symmetric infinitely thin shell, bounded by two Schwarzschild vacuum regions, will be recalled.

2.1. Equation of motion

Consider now a single shell and assume that the metric of the Schwarzschild regions on the sides of the shell**, signified by '−' and '+',** is given as

$$\mathrm{d}s_{\pm}^2 = -f_{\pm}(r)\,\mathrm{d}t_{\pm}^2 + f_{\pm}(r)^{-1}\mathrm{d}r^2 + r^2\,(\mathrm{d}\vartheta^2 + \sin^2\vartheta\,\mathrm{d}\varphi^2), \tag{2.1}$$

were **the indices ± signifies the outer and inner regions, respectively,** r stands for the area radius, which is assumed to be continuous across the shell, t_- and t_+ denote the Schwarzschild time coordinates in the corresponding spacetime regions, ϑ and φ are the standard spherical coordinates, while

$$f_{\pm}(r) = 1 - \frac{2M_{\pm}}{r} \tag{2.2}$$

with mass parameters $M_\pm$, respectively ‡.

Denote by u^a the four-velocity tangent to the timelike generators of the shell and by τ the proper time along these timelike generators. The **coordinate basis** components of u^a can be given as

$$u^\alpha_\pm = \left(\frac{\mathrm{d}t_\pm}{\mathrm{d}\tau}, \frac{\mathrm{d}r}{\mathrm{d}\tau}, 0, 0\right) . \tag{2.3}$$

The induced metrics, h^-_{AB} and h^+_{AB}, on the mutual boundary of the two spacetime regions, are assumed to coincide, and the metric on the shell $h_{AB} = h^+_{AB} = h^-_{AB}$, in the $(\tau, \vartheta, \varphi)$ coordinates, reads as

$$h_{AB} = \mathrm{diag}(-1, r^2(\tau), r^2(\tau)\sin^2\vartheta) . \tag{2.4}$$

As the four-velocity u^a is of unit norm its components are not independent and, in virtue of (2.1) and (2.3), the relations $u_a u^a = -1$ implies that the relation

$$\left(f_\pm \frac{\mathrm{d}t_\pm}{\mathrm{d}\tau}\right)^2 = f_\pm + \left(\frac{\mathrm{d}r}{\mathrm{d}\tau}\right)^2 \tag{2.5}$$

holds from which, with the inclusion of the sign factor $\epsilon_{t_\pm} = \mathrm{sign}(f_\pm \cdot \mathrm{d}t_\pm/\mathrm{d}\tau)$,

$$\frac{\mathrm{d}t_\pm}{\mathrm{d}\tau} = \frac{\epsilon_{t_\pm}\sqrt{f_\pm(r) + (\mathrm{d}r/\mathrm{d}\tau)^2}}{f_\pm(r)} , \tag{2.6}$$

can be deduced. We shall return to the fixing of this sign factor later in Subsection 2.5. Nevertheless, let us mention here only that the value of ϵ_{t_-} or ϵ_{t_+} is $+1$ in regions where t_- or t_+ is a timelike coordinate, i.e. above the respective horizons.

The unit normal n_a to the shell, satisfying the orthogonality requirement $u^a n_a = 0$, **is chosen then as follows. The ancestors of n_a in advance to the matching, the unit normals $n_{a\pm}$ to the respective boundaries Σ_- and Σ_+ deviding the '$-$' and '$+$' spacetimes into two parts—as it is indicated by the schematic figure Fig.1**—can be given as

$$n_{\alpha\pm} = \epsilon_{n_\pm}\left(-\frac{\mathrm{d}r}{\mathrm{d}\tau}, \frac{\mathrm{d}t_\pm}{\mathrm{d}\tau}, 0, 0\right) , \tag{2.7}$$

where the value of the sign factor $\epsilon_{n_\pm}$ **depends on the choices made for the regions to be matched. is chosen such that n_a points outward as it is illustrated in Fig.1. In the particular Schwarzschild case this implies that $\epsilon_{n_\pm} = +1$.** §

Correspondingly, in carrying out a mathching first separate choices for either of the sides of the boundaries Σ_- and Σ_+ dividing the '$-$' and '$+$'

‡ Note that the form of the metric (2.1) with the slightly more generic metric function $f_\pm(r) = 1 - 2M_\pm(r)/r$ is suitable to cover, beside the Schwarzschild metric that of the de Sitter spacetime in the vacuum case, or whenever electrovacuum spacetimes are also included the Reisner–Nordström de Sitter solutions do also fit to this form.

§ **Note that by allowing $\epsilon_{n_\pm}$ to take the value ± 1 within the very same setup wormholes [16, 17] and other type of exotic spacetimes can be studied. However, in this paper attention will be restrected to conventional shells exclusively.**

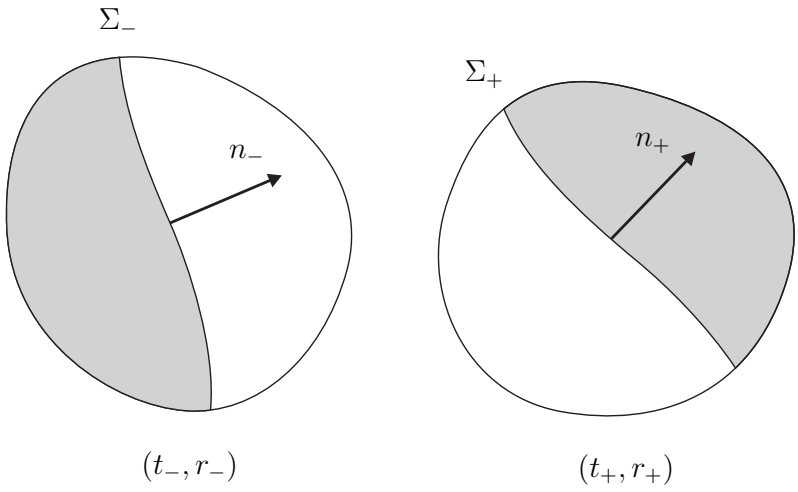

Figure 1. **The freedom related to the choices of the parts of the separated '−' and '+' spacetimes is indicated. In each of these regions one of the signified vectors corresponds to $\epsilon_{n_\pm} = 1$, while the vector pointing to the opposite direction comes with $\epsilon_{n_\pm} = -1$. The convention applied for fixing the sign of $\epsilon_{n_\pm}$ is illustrated. The regions to be matched are indicated by the grey domains while $\Sigma_\pm$ denotes their 'isometric' boundaries in the preliminary spacetimes.**

spacetimes into two parts have to be done. These are the sides to be matched indicated by the gray regions in Fig.1. Once this choice has been made the values of ϵ_{n_-} and ϵ_{n_+} gets to be determined by the following orientation rule. To have a well-defined normal vector field n_a after the matching had been made the normal vectors, n_{a-} and n_{a+}, are required to be oriented such that n_{a-} points outward from the '−' region, while n_{a+} points inward in the '+' region. Accordingly, the values of ϵ_{n_-} and ϵ_{n_+} get to be completely fixed after the choices for the subregions of the '−' and '+' spacetimes is made.

Now, with the help of the induced metric, h_{AB}, and the unite normal $n_{a\pm}$ the extrinsic curvature tensors, at the boundaries Σ_- and Σ_+, are given as

$$K^{\pm}_{AB} = \frac{1}{2} h_A{}^E h_B{}^F \pounds_{n_\pm} h_{EF} \,. \tag{2.8}$$

As already mentioned the equation of motion for the shell separating the Schwarzschild regions can be derived in various ways. One of the most frequently applied method is based on Israel's thin-shell formalism [31] in which junction conditions are specified at the location of the shell. In particular, besides the relation $h_{AB} = h^+_{AB} = h^-_{AB}$ the discontinuity of the pertinent extrinsic curvature tensors, K^+_{AB} and K^-_{AB}, are assumed to be related to the surface energy-momentum tensor of the shell $S_{AB} = \mathrm{diag}(\sigma, \mathcal{P}\cdot r^2, \mathcal{P}\cdot r^2 \sin^2\theta)$—where σ and $\mathcal{P}$ denote the surface energy density and the 2-dimensional tangential pressure of the shell, respectively—via the Lanczos equation

$$K^+_{AB} - K^-_{AB} = -8\pi \left\{ S_{AB} - \frac{1}{2} h_{AB} \left(h^{CD} S_{CD} \right) \right\} . \tag{2.9}$$

By making use of (2.7) and (2.8) we get that $K^{\pm}_{\vartheta\vartheta} = \epsilon_{n_\pm} r f_\pm(\mathrm{d}t_\pm/\mathrm{d}\tau)$. Then, in virtue of (2.9), the ϑ-ϑ component of this junction condition can be seen to take the form

$$s_- \sqrt{f_-(r) + \left(\frac{\mathrm{d}r}{\mathrm{d}\tau}\right)^2} - s_+ \sqrt{f_+(r) + \left(\frac{\mathrm{d}r}{\mathrm{d}\tau}\right)^2} = 4\pi\sigma r\,, \tag{2.10}$$

where now r signifies the radius at the location of the shell, while the sign factors s_- and s_+ are nothing but the products of $\epsilon_{t_\pm}$ and $\epsilon_{n_\pm}$, i.e. $s_\pm = \epsilon_{t_\pm}\epsilon_{n_\pm}$. **Since $\epsilon_{n_\pm} = +1$, $s_\pm = \epsilon_{t_\pm}$ hereafter.**

Note that the importance of the appropriate treatment of the sign factors s_- and s_+—**as it** was **already** emphasized in [33, 34] **is of fundamental importance—can be done as follows. Suppose that we start by specifying the mass parameters of the matched spacetime regions. Then, in each of these Schwarzschild spacetimes there is a closed hypersurface deviding the spacetime into two disjoint regions. Accordingly, we always have four different choices—the two inner and two outer regions—to be matched, as it is indicated by Fig.1. Note that the mass parameters are not informative in carrying out the corresponding decision and this is the very ambiguity indicated by the use of the sign factors s_- and s_+ in (2.10). The value of these factors is restricted only by the expectation that the rest mass of the shell $m_r = 4\pi\sigma r^2$ be non-negative. Thereby, if we have only a single shell, in conventional situations, when an inner Schwarzschild region with smaller mass parameter is matched to an outer Schwarzschild region both s_- and s_+ are equal to $+1$. These type of shell are going to be referred as conventional Schwarzschild shells. If either of these regions is replaced by its complement then the corresponding sign factor has to be replaced by its opposite. For instance, when two outer regions are identified $\epsilon_{n_-} = -1$ while $\epsilon_{n_+} = 1$ and the yielded spacetime describe the motion of a shell in a wormhole spacetime [16, 17], which, provided that the inequality $M_- \leq M_+$ holds for the Schwarzschild masses of the matched regions, implies that σ and, in turn, m_{r} have to be negative for wormhole configurations. We do not intend to consider these type of configurations, i.e. in the rest of this paper we assume that both ϵ_{n_-} and ϵ_{n_+} will always take the value $+1$. Note that this does not exclude the appearance of non-conventional matchings which will occur, for instance, whenever the motion of multi-layer shell systems is considered and shell crossings are also allowed to happen there may arise situations in which ϵ_{t_+} changes sign and the mass parameter of the developing intermediate region gets to be larger than that of the outermost region. As we shall see in Subsection 4.3 (see also [36]), this implies that the gravitational mass of one of the shells becomes negative and this always happens in situations where mass inflation occurs.**

In returning to the main line of our argument, it is worth to be emphasized that regardless of the values of these sign factors in the energy balance relation (2.10) or, more importantly, Regardless which of the alternative methods, mentioned in the introduction, is applied the reasonings always end up with the equation of motion

$$\left(\frac{\mathrm{d}r}{\mathrm{d}\tau}\right)^2 = \left(\frac{m_\mathrm{g}}{m_\mathrm{r}}\right)^2 - 1 + \frac{2m_\mathrm{c}+m_\mathrm{g}}{r} + \left(\frac{m_\mathrm{r}}{2r}\right)^2 , \tag{2.11}$$

where $m_\mathrm{c} = M_-$ denotes the Schwarzschild mass parameter of the central region, $m_\mathrm{r} = 4\pi\sigma r^2$ is the 'rest mass' of the shell representing the surface internal energy associated with the tangential motion of particles, while $m_\mathrm{g} = M_+ - M_-$ is the 'gravitational mass' of the shell **defined such that $m_\mathrm{c}+m_\mathrm{g}$ is the mass parameter of the exterior Schwarzschild region**. Accordingly, m_c and m_g are constants but in general m_r is function of the radius, and it is constant only in the particular case of dust shells with zero pressure.

To determine the r-dependence of m_r we need an additional equation which can be derived by making use of the conservation law $D^A S_{AB} = 0$, where D_A denotes the covariant derivative **associated** with the metric h_{AB}. In this particular case the conservation law takes the form [36] ‖

$$\frac{\mathrm{d}}{\mathrm{d}\tau}\left(\sigma r^2\right) = \mathcal{P}\frac{\mathrm{d}}{\mathrm{d}\tau}\left(r^2\right) , \tag{2.12}$$

By introducing the area radius r, instead of τ, as our independent variable (2.12) can be put into the form

$$r\frac{\mathrm{d}\sigma}{\mathrm{d}r} = -2(\sigma+\mathcal{P}) . \tag{2.13}$$

This is the point where the EOS of the shell comes into play. With the help of an EOS of the form $\mathcal{P} = \mathcal{P}(\sigma)$ the functional form of $\sigma = \sigma(r)$ may be determined, which, in turn, gives us the functional form of $m_\mathrm{r}(r)$, as well. Since (2.13) is a separable differential equation an implicit solution to it—provided that the EOS is regular enough to guarantee the above integral to exist—can be written as

$$\frac{r}{r_0} = \exp\left(-\frac{1}{2}\int_{\sigma_0}^{\sigma(r)} \frac{\mathrm{d}\tilde{\sigma}}{\tilde{\sigma}+\mathcal{P}(\tilde{\sigma})}\right) , \tag{2.14}$$

with integration constant $\sigma_0 = \sigma(r_0)$.

Once $m_\mathrm{r}(r)$ is known (2.11), along with suitable chosen initial conditions, can be used to determine the motion of as a function of the proper time τ.

‖ (2.12) may also be derived by making use of the two algebraically independent components of (2.9).

2.2. Equation of state

Although the developed C++ code allows us the use of basically any kind of EOS in the numerical investigations covered by this paper only the homogeneous linear EOS is applied. It is also important to keep in mind that in specifying an EOS some additional restrictions are always needed to be taken into account. For instance, the use of a suitable energy condition is essential. The most appropriate one is the so called dominant energy condition (DEC) guaranteeing that solutions to dynamical problems do respect the concept of causality. For a selected type of infinitesimally thin shell DEC can be seen to hold whenever $|\mathcal{P}| < \sigma$, which, in particular, means that σ is non-negative (see, e.g., [8, 54]). To avoid dynamical instabilities we shall also assume that the square of the speed of sound, $c_{\mathrm{s}}^2 = \mathrm{d}\mathcal{P}/\mathrm{d}\sigma$, is non-negative, and to be compatible with the conventional concept of relativity, that c_{s}^2 is less than or equal to the square of the speed of light.

As mentioned above, for the shake of simplicity, in this paper considerations will be restricted to the simplest possible functional form, i.e. to a homogeneous linear EOS $\mathcal{P}(\sigma) = w\sigma$ in which case (2.14) takes the form

$$\sigma(r) = \sigma_0 \left(\frac{r}{r_0}\right)^{-2(1+w)} . \tag{2.15}$$

DEC, along with hydrodynamical stability on the surface, can be seen to hold whenever w is chosen from the interval $[0, 1]$ $0 \leq w \leq 1$. Note also that $w = 0$ corresponds to the dust case.

2.3. Initial conditions

In applying Israel's junction conditions **in practice either of the following two approaches manifest itself. O**one may start by fixing the geometrical properties of the spacetimes on the respective sides of the shell and then solve the junction conditions for suitable rest mass and initial velocity values making the matching to be possible. This could be referred as **the a** 'mathematician approach', while in **the a** 'physicist approach' one would start by fixing the rest mass and initial velocity of the shell and then try to determine suitable geometrical parameters of the respective side spacetime regions. Below this latter approach is applied.

Accordingly, in describing the motion of a shell we regard m_{c} as environmental parameter and m_0, r_0, v_0 as initial parameters of the shell at τ_0. **With these parameters Here** $m_0 = m_{\mathrm{r}}(r_0)$, $r_0 = r(\tau_0)$, $v_0 = \dot{r}(\tau_0)$, and the over-dot denotes derivative with respect to the proper time, τ. As mentioned above to be compatible with DEC we shall assume that $m_0 > 0$. In virtue of equation (2.11), or (2.10), whenever the junction is possible to be done the gravitational mass, m_{g}, depends only on the kinetic energy and it may be expressed in terms of the initial data as

$$m_{\mathrm{g}} = m_0 \left(-\frac{m_0}{2r_0} + \epsilon_{\mathbf{g}} \sqrt{1 - \frac{2m_{\mathrm{c}}}{r_0} + v_0^2}\right) . \tag{2.16}$$

where ϵ_g stands for the indication of another sign ambiguity which will be discussed below (see Table 2.3.).

In order to avoid the gravitational mass to become complex the inequality

$$v_0^2 \geq \frac{2m_c}{r_0} - 1 \tag{2.17}$$

has to hold. **Note that in choosing v_0 beside (2.17), in general, some of the following additional conditions are also needed to be taken into account. Assuming that $m_0 > 0$, the sufficient conditions ensuering the existence of the desired type of matching, depending on the four possible choices for the signs s_- and s_+, along with the pertinent values of ϵ_g in (2.16) and the respective signs of m_g are indicated in Table 2.3**

In virtue of (2.16) m_g may be negative. Note also that since σ is required to be positive $\epsilon_{t_-} = -1$ and $\epsilon_{t_+} = +1$ cannot occur. As we shall see below (2.26) excludes the possibility of having both ϵ_{t_-} and ϵ_{t_+} to be negative. Thus, in the remaining two cases, the sufficient conditions ensuring the existence of the desired type of matching are given as

ϵ_{t_-}	ϵ_{t_+}	sufficient conditions	gravitational mass
$+$	$+$	$v_0^2 > A$	$m_g > 0$
$+$	$-$	$v_0^2 < A$	$m_g > 0$, if $v_0^2 > B$ $m_g \leq 0$, elsewhere .

Table 1. The value of ϵ_g, along with the corresponding sign of m_g, is given with respect to the sufficient conditions ensuering the existence of the desired type of matchings.

where

$$A = \frac{m_0^2}{r_0^2} + \frac{2m_c}{r_0} - 1\,, \tag{2.18}$$

$$B = \frac{m_0^2}{4r_0^2} + \frac{2m_c}{r_0} - 1\,. \tag{2.19}$$

Note that (2.17) do also ensure that in (2.10) neither of the terms involving square roots will be complex. In fact, (2.17) guarantees that the first term in (2.10) will not be complex, while by making also use of (2.16) the second term can also be seen to be non-complex. Whenever $m_g < 0$ neither of the terms in (2.10) could become complex.

We would also like to emphasize that, as the right hand sides of (2.17), (2.18) and (2.19) tend to -1 while $r_0 \to \infty$, for sufficiently large value of r_0 therefore in some cases there is no restriction on the initial velocity. For instance, define

$$r_A = m_c + \sqrt{m_c^2 + m_0^2}\,, \tag{2.20}$$

which is the solutions to $A = 0$. Then, we get that for a conventional shell v_0 is arbitrary if $r_0 \geq r_A$.

We would also like to mention that the need for the use of analogous conditions was noticed in [47]. More concretely, it was claimed in [47] that a shell, in the particular case with $m_c = 0$, cannot be in rest below its own event horizon, i.e. whenever $r < 2m_g$. By making use of (2.10) a statement—generalizing this claim of [47]—justifying that the minimal radius of the shell in rest cannot to be smaller than the Schwarzschild radius, $R_s = 2(m_c + m_g)$, of the external spacetime region can be seen to be true for arbitrary value of m_c as for a shell in rest with $s_- = +1$ and $s_+ = +1$ for the metric function $f_\pm > 0$ must hold. By applying (2.20), with the substitution of $v_0 = 0$ and $r_0 = r_A$ to (2.16), the Schwarzschild radius as a generic lower bound can be justified to be sharp.

2.4. Characterizing the dynamics

For dust shells the values of m_g **and, along with that of m_r—it the latter** is also constant **in this particular case for dust shells**—, characterizes the motion in the following way. The system is said to be gravitationally bound whenever there exists a finite radius, r_{max}, such that the velocity vanishes at r_{max}. In general, the value of r_{max} coincides with the positive root of the right hand side of (2.11) which, whenever $m_g < m_r$ reads as ¶

$$r_{max} = \left(1 - \frac{m_g^2}{m_r^2}\right)^{-1} \left(m_c + \frac{m_g}{2} + \sqrt{m_c^2 + m_c m_g + \frac{m_r^2}{4}}\right). \tag{2.21}$$

If $m_g = m_r$ the kinetic energy gets to be zero exactly at the spatial infinity, i.e. whenever $r_{max} = \infty$, and the associated motion is usually referred as 'marginally bound'. For $m_g > m_r$ the motion of the shell is not restricted, and, in virtue of (2.16), at the spatial infinity, i.e. in the $r_0 \to \infty$ limit, the relation $m_g = m_r\sqrt{1 + v_\infty^2}$ holds.

Although the solution to (2.11) is **too, in general,** complicated **in the generic case**, for dust shells it can be given in closed form (see, e.g, [47]). For example, in the special case of marginally bound motion, with $m_g = m_r$, the pertinent solution can be given by the implicit relation

$$\tau(r) = \left.\frac{(4\tilde{r}m_c + 2\tilde{r}m_r - m_r^2)\sqrt{8\tilde{r}m_c + 4\tilde{r}m_r + m_r^2}}{24m_c^2 m_r^2}\right|_{\tilde{r}=r}^{\tilde{r}=r_0}, \tag{2.22}$$

where r_0 denotes the initial location of the shell at $\tau = 0$. Setting $r_0 = 0$ the value of $-\tau(r)$ gets to be equal to the proper time lasting meanwhile the shell collapses from radius r to the symmetry center. Specializing even further, for a 'self-gravitating' shell

¶ It follows from (2.21) that $r_{max} \geq R_S = 2(m_c + m_g)$ as mentioned before.

with Minkowski interior, i.e. with $m_{\mathrm{c}} = 0$, the proper time that is needed for such a shell of radius r to undergo a complete gravitational collapse can be given as

$$\tau_{\mathrm{c}}(r) = \frac{m_{\mathrm{r}}}{6} + \frac{\sqrt{4r + m_{\mathrm{r}}}}{3}\left(\frac{r}{\sqrt{m_{\mathrm{r}}}} - \frac{\sqrt{m_{\mathrm{r}}}}{2}\right). \tag{2.23}$$

It is worth keeping in mind that the above analytic expressions were derived by making use of the assumption that the motion is marginally bound which, in particular, means that the velocity of the shell at r is supposed to be as if the shell started to move towards the center from rest at spatial infinity.

For shells with non-zero pressure, the situation is more complex because pressure may, and in fact do, significantly alter the motion of the particles. By investigating the case of homogeneous linear EOS it was justified, in contrast to the dust case, that such a shell may be in equilibrium, although the pertinent equilibrium was found to be unstable [55, 37]. More complicated EOS such as polytrop can only be studied numerically, and—as it was justified by our numerical experiences (for details see [56])—it is always possible to construct shells, which do oscillate in a bounded region or which are in stable equilibrium.

2.5. The Schwarzschild time and the Eddington–Finkelstein null coordinates

Up to this point all the derivatives in the equations relevant for the evolution of the investigated shell were expressed with respect to the proper time associated with the shell. In many practical cases it turns out to be necessary—as it will be clearly demonstrated in the following sections concerning the collision of shells—to know what is the functional relation of this proper time, e.g., to the Schwarzschild time coordinates defined on the inner and outer sides of the shell. We would like to emphasize that in the applied formalism only the area radius, r, is required to be a continuous—although, not necessarily monotonous—function through the shells. Accordingly, in general the Schwarzschild time coordinates defined on the sides need not match to each other continuously. Therefore, we have to determine the functional relation of the proper time to both the inner and outer Schwarzschild time coordinates, separately.

In doing so recall that the derivative $(\mathrm{d}t_{\pm}/\mathrm{d}\tau)$ has been given by (2.6). Note, however, that the value of $\epsilon_{t_{\pm}}$—for its definition see Subsection 2.1—is undetermined yet, although it is uniquely determined in regions where the Schwarzschild time coordinates increase in the future direction, i.e. whenever the radius is larger than both of the Schwarzschild–radius, as then $\mathrm{d}t_{\pm}/\mathrm{d}\tau > 0$ and $f_{\pm} > 0$ excludes requires the use of $\epsilon_{t_{\pm}} = -+1$ in (2.6).

Nevertheless, as it was shown in [36] the derivative $(\mathrm{d}t_{\pm}/\mathrm{d}\tau)$ can always be determined uniquely. More concretely, by making use of the $\tau - \tau$ component of (2.9) it can be shown—for details see, e.g., the part of Section 2 in [36] between equations (2.21) and (2.34)—that regardless of the location of the shell, whenever it moves in a

Schwarzschild spacetime

$$\frac{\mathrm{d}t_-}{\mathrm{d}\tau} = \left(1 - \frac{2m_\mathrm{c}}{r}\right)^{-1} \left(\frac{m_\mathrm{g}}{m_\mathrm{r}} + \frac{m_\mathrm{r}}{2r}\right) , \tag{2.24}$$

$$\frac{\mathrm{d}t_+}{\mathrm{d}\tau} = \left(1 - \frac{2(m_\mathrm{c}+m_\mathrm{g})}{r}\right)^{-1} \left(\frac{m_\mathrm{g}}{m_\mathrm{r}} - \frac{m_\mathrm{r}}{2r}\right) , \tag{2.25}$$

or equivalently, the relations $\epsilon_{t_\pm}\sqrt{f_\pm(r)+(\mathrm{d}r/\mathrm{d}\tau)^2} = m_\mathrm{g}/m_\mathrm{r} \mp m_\mathrm{r}/2r$ are always satisfied everywhere. This, in particular, implies that

$$\epsilon_{t_\pm} = \mathrm{sign}(m_\mathrm{g}/m_\mathrm{r} \mp m_\mathrm{r}/2r) \,,. \tag{2.26}$$

and, in virtue of (2.16), the relation $\epsilon_\mathrm{g} = \epsilon_{t_-}$ also follows.

It follows from (2.26) that **depending on the sign of m_g only** either ϵ_{t_-} or ϵ_{t_+} **might do** change sign **depending on the sign of m_g. The location of this sign change is referred as the 'critical radius' the value of which is given as $\widehat{r} = |m_\mathrm{r}^2/(2m_\mathrm{g})|$. This sign change happens at the 'critical radius' $\widehat{r} = m_\mathrm{r}^2/(2|m_\mathrm{g}|)$.** [+]

Once the initial values for t_- and t_+ are specified, these equations determine the desired relations between the proper time and the Schwarzschild time coordinates in the inner and outer spacetime regions, respectively. The differences of the right hand sides of (2.24) and (2.25) make it clear that, apart from very exceptional cases, even though the initial values for t_- and t_+ **at a certain position of the shell would be are** chosen to coincide they will necessarily differ latter, i.e. they need not match continuously as it was indicated above.

Since The Schwarzschild metric has a coordinate singularity at the event horizon, i.e. at $r = 2m_\mathrm{c}$ **in the inner region and at $r = 2(m_\mathrm{c}+m_\mathrm{g})$ in the outer region. , corresponding to infinite value of** The Schwarzschild time coordinate**gets to be infinite while approaching the horizon, thereby**, it does not allow the proper description of the motion **below through** the horizon. It is possible to overcome this technical difficulty by applying **the** ingoing Eddington–Finkelstein coordinates covering both the domain of outer communication and the black hole regions simultaneously. The ingoing Eddington–Finkelstein null coordinate is defined as $\mathrm{v}_\pm = \mathrm{t}_\pm + \mathrm{r}^*$, where r^* denotes the 'tortoise coordinate' determined by the relation $\mathrm{d}r^*/\mathrm{d}r = f_\pm^{-1}(r)$. Accordingly,

$$\frac{\mathrm{d}\mathrm{v}_\pm}{\mathrm{d}\tau} = \frac{\mathrm{d}t_\pm}{\mathrm{d}\tau} + \frac{\mathrm{d}r^*}{\mathrm{d}r}\frac{\mathrm{d}r}{\mathrm{d}\tau} = \frac{\epsilon_{t_\pm}\sqrt{f_\pm(r)+(\mathrm{d}r/\mathrm{d}\tau)^2}+\mathrm{d}r/\mathrm{d}\tau}{f_\pm(r)} , \tag{2.27}$$

where $\epsilon_{t_\pm}$ is given by (2.26).

It is possible to determine the value of the sign factor $\epsilon_{t_\pm}$ in front of the square root on the right hand side of (2.27) as, in each of the regions, the

[+] Note that whenever $\mathcal{P} \geq 0$ the value of $\widehat{r}$ is unique due to the monotonicity of the functions $m_\mathrm{r} = m_\mathrm{r}(r)$. It can also be checked that unless this change of the sign happened the worldsheets representing the evolving shells **cancould** not be of class C^2 at $r = \widehat{r}$.

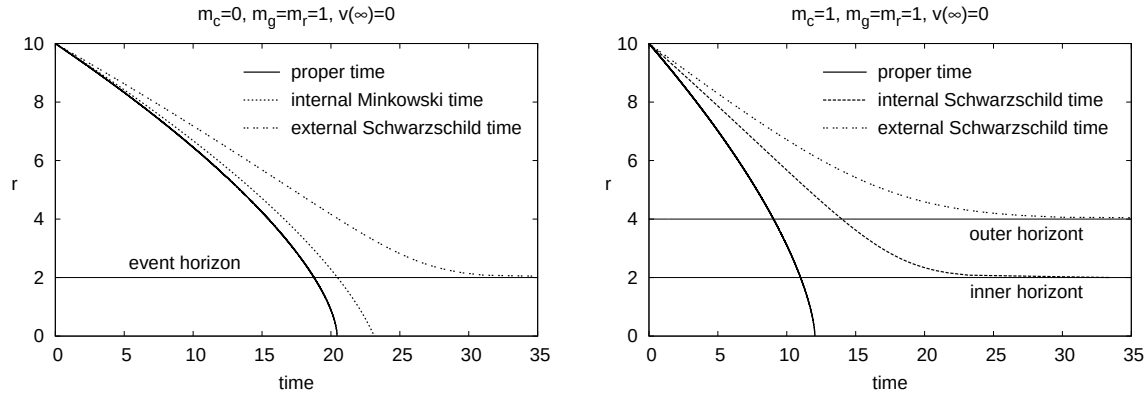

Figure 2. On the left panel the motion of a single dust shell, starting at $r = 10$, in the particular case with $m_{\rm c} = 0$, $m_{\rm r} = m_{\rm g} = 1$ is shown with respect to the proper time, the interior Minkowski time and the exterior Schwarzschild time. In the last case, as it is indicated by the pertinent plot, the shell can only asymptotically reach the event horizon, while the time of complete collapse is $\tau_{\rm c} = (19\sqrt{41}+1)/6 \approx 20.44$ or $t_{\rm c} = (11\sqrt{41}-1)/3 \approx 23.14$ with respect to the proper or inner Minkowski time, respectively. On the right panel the motion of a similar shell with $m_{\rm c} = m_{\rm r} = m_{\rm g} = 1$ is indicated. In this case the inner and outer horizons denote the horizons at the central and exterior Schwarzschild regions, respectively.

value of $v_\pm$ must increase along the generators of the the evolving shell which are future directed timelike curves. Therefore, the left hand side of (2.27) must be non-negative everywhere. Since the $r = const$ hypersurfaces are spacelike in the black hole region $\mathrm{d}r/\mathrm{d}\tau$ has to be non-positive there, as well. Thus, $\mathrm{d}r/\mathrm{d}\tau$ may be replaced by $-|\mathrm{d}r/\mathrm{d}\tau|$ and then, by demanding continuity through the horizon, where $f_\pm(r) = 0$, it can be seen that $\epsilon_{t_\pm}$ has to take the value $+1$ on the black hole region side. Hence, the value of ϵ_t must be $+1$ both in the domain of outer communication and the black hole region side. Note that this argument, concerning the sign fixing of $\epsilon_{t_\pm}$, does not apply if the shell starts its motion inside the black hole region as then the continuity at the event horizon cannot be used as a guiding principle.

Note that in the particular case of a dust shell with $m_{\rm c} = 0$ and $m_{\rm g} = m_{\rm r}$, by making use of (2.24) and (2.23), the time needed for **the a** complete gravitational collapse may be given in terms of the interior Minkowski time as

$$t_{\rm c}(r) = \frac{\sqrt{4r + m_{\rm r}}}{3}\left(\sqrt{m_{\rm r}} + \frac{r}{\sqrt{m_{\rm r}}}\right) - \frac{m_{\rm r}}{3}\,. \tag{2.28}$$

In closing this section we would like to emphasize that in describing the motion of a single shell—**that is governed determined** by (2.11)—only the mass parameters of the interion and exterior Schwarzschild spacetime regions, along with the mass of the shell (which **is determined by depends on** the surface energy density**, along with and** the pertinent EOS of the shell) that count. In particular, **as far as no collision between a selected and the surrounding shells happen** the motion

of **a the selected one shell is insensitive whether depends only on** the mass parameters of the interior and exterior **Schwarzschild** regions **are produced be a single object such as a Schwarzschild black hole or by a series of shells similar to the investigated one on both sides provided that no collision between the selected and surrounding shells happen.** Note also that likewise in the Newtonian case the mass of the interior shells (if they exist at all) comes into play only via the value of the central mass $m_{\rm c}$. However, as the gravitational mass $m_{\rm g}$ may not be positive**,** the general relativistic motion of the shell may differ significantly from that of a shell, possessing the same $m_{\rm c}$ and $m_{\rm r}$ parameters, **described** in the Newtonian theory.

2.6. The motion of shells in the Newtonian case

In this section, for the sake of completeness and for comparison, first a brief review of the **description of dust shells in the** Newtonian framework will be given. Then, the equations of motion will be **extended in order to be able to include shells made of fluid in this setup derived for fluid shells**. Throughout this subsection**, for clear distinction,** the basic quantities in the Newtonian framework will be signified by upper case letters corresponding to the ones introduced in the previous sections for fully relativistic systems.

To start off Note first that in the Newtonian theory the inertial mass and the gravitational mass of a shell are not distinguished. **, therefore** This common mass of the shell—which, in the Newtonian description, is independent of time and the EOS— will be denoted by $M_{\rm shell}$. The other considerable simplification characterizing the Newtonian theory comes from the use of absolute time, denoted by T.

Likewise in the fully relativistic case the equation of motion of the shells in the Newtonian framework can be derived in various ways. In case of dust shells, i.e. for shells with zero pressure, a good review can be found in [57]. According to the argument outlined therein the basic equation is nothing but a ballance equation of force per unit mass and for the dust case it possesses the form of (2.29) below with $P = 0$.

In generalizing this result to the fluid **case shells**, i.e. in determining the functional form of the last term on the right hand side of (2.29) with $P \neq 0$, we need to find the appropriate force term representing the contribution of the pressure to the Newtonian ballance equation. In identifying it let us consider an elementary 'square shaped' surface element of the shell with sides $R\,\Delta\phi$, where $\Delta\phi$ denotes the viewing angle of the sides from the center. The mass of this elementary piece is $\Delta M_{\rm shell} = \Sigma\, R^2(\Delta\phi)^2$, where $\Sigma = M_{\rm shell}/(4\pi R^2)$ is the surface mass density. There are four elementary forces exerted at the sides of this square shaped surface element. The size of these elementary forces is $\Delta F = P\, R\, \Delta\phi$, where P denotes the 'two-dimensional' pressure of the shell. Since the direction of these forces are tangential to the shell the resultant total force is radially outwards pointing and its size is $\Delta F_{\rm tot} = 4\Delta F \sin(\Delta\phi/2)$. Correspondingly, $\Delta F_{\rm tot}$ tends to $2\Delta F\Delta\phi$ in the $\Delta\phi \to 0$ limit which, in turn, justifies that the force per unit mass, due to the non-zero pressure, is $\lim_{\Delta\phi\to 0} \Delta F_{\rm tot}/\Delta M = 8\pi PR/M_{\rm shell}$. Accordingly, the

equation of motion is of the form

$$\ddot{R} = -\frac{2M_{\rm c} + M_{\rm shell}}{2R^2} + \frac{8\pi PR}{M_{\rm shell}} \tag{2.29}$$

and the initial condition to this differential equation consits of $M_{\rm shell}$, R_0 and V_0, where $V_0 = {\rm d}R/{\rm d}T$ at R_0. In addion, as in the relativistic case, we need the central mass, $M_{\rm c}$, as environmental variable. Formally the gravitational mass can be calculated from the initial conditions just as in Einstein theory, but, as we noted above, in this case the gravitational mass has to coincide simply with $M_{\rm shell}$. In comparing results relevant for the Newtonian and Einstein theories we need to harmonize initial conditions. Note that while r_0 and R_0, or v_0 and V_0, have identical interpretations in both theories, in setting the value of $M_{\rm shell}$ we have the following inequivalent two choices. We may identify $M_{\rm shell}$ with either the rest mass or the gravitational mass in the Einsteinian setup. As in the Newtonian regime, i.e. whenever $r_0 \gg m_{\rm c}, m_{\rm g}$ and $v_0 \ll 1$, the relation $m_{\rm g} \sim m_{\rm r}$ holds we could identify either of them with $M_{\rm shell}$. Nevertheless, as conceptionally the gravitational mass plays the same role in both theories it seems to be more appropriate to assume the equality of the two gravitational masses by setting $M_{\rm shell} = m_{\rm g}$.

Assuming that P is a given function of the radius, $P = P(R)$, the equation of motion, (2.29), can be integrated. The existence of such a function is always guaranteed whenever an EOS of the form $P = P(\Sigma)$ is known because $\Sigma = M_{\rm shell}/(4\pi R^2)$ itself is a function of the radius. It is worth to be emphasized that the EOS was kept to be completely generic throughout the above discussion.

Multiplying (2.29) by $\dot{R}$ and then by integrating with respect to T one gets, as the analog of (2.11), the Newtonian energy balance equation

$$\dot{R}^2 = V_0^2 + \left[\frac{2M_{\rm c} + M_{\rm shell}}{\tilde{R}}\right]_{R_0}^{R} + 4\int_{R_0}^{R} \frac{W(\tilde{R})}{\tilde{R}}{\rm d}\tilde{R}\,, \tag{2.30}$$

where $W(R) = P(R)/\Sigma(R)$. In particular, in case of shell with a linear EOS where $W(R) = \overline{W} = const$, the last term at the right hand side of (2.30) takes the form $4\overline{W}\ln(R/R_0)$.

3. The evolution of multi-layer shell systems

This section is to provide a brief review of the analytic and numerical setup we have applied in studying the evolution of multi-layer shell systems. This evolution, in general, involves a large number of collisions of the shells. **Two of the basic types of pairwise collisions are discussed in the following Subsection.**

3.1. Collisions of two shells

As it was emphasized in Section IV of [57] the description of a collision of two shells cannot be done without invoking some further assumptions concerning the interaction of the shells. More concretely, there is an ambiguity in the evolution of colliding shells even

though the energy and momentum conservations are guaranteed to hold as—depending on the type of interactions of the shells—more than two shells or even a continuous spread of the matter of the original two shells into a thick shell might develop during the collision.

This ambiguity gets to be eliminated if the two shells pass through each other either without any interaction, in this case the collision is said to be *totally transparent*, or when the interaction is extremely strong and the ingoing shells merge into a single outgoing shell, in which case the collision is referred as *totally inelastic*. **This section is to recall the basic relations which can be applied in case of totally transparent and totally inelastic collisions. It is important to emphasize that although between** These two extreme cases—**which** are schematically represented by Fig. 3.—**there are plenty other possible collisions yielding exactly two outgoing shells, nevertheless, without making further assumptions about the interchange of their matter content, in particular, the changes of their EOS, the evolution of these outgoing shells cannot be uniquely determined. In this paper only the totally transparent shell crossings will be considered. The EOS of the shells will also be assumed to be intact in collisions. Note that while for dust shells this assumption seems to be appropriate it is much less adequate whenever the shells are comprised by strongly interacting particles. Below the basic equations relevant for totally transparent collisions are recalled.** *

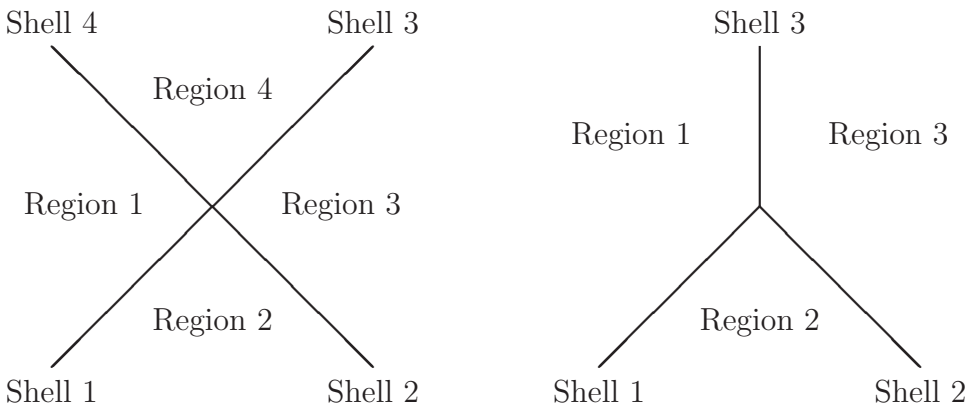

Figure 3. Schematic spacetime diagrams representing the totally transparent (left) and totally inelastic (right) collisions. The vertical direction is temporal and time progresses upward.

The totally transparent collision could be modelled by the crossing of two dust shells the particles of which do not have other than gravitational interaction both during their separate motion and also when they are passing through each other. Detailed investigation of the dynamics of totally transparent collision **of two shells** can be found in [36]. For this type of collision it is assumed

* **A detailed analytic description of the totally inelastic case has been given in the appendix [8] while the C++ code [52] is developed such that it is capable to investigate the evolution of shell systems when the collisions are assumed to be totally inelastic.**

that $m_{\mathrm{r}3} = m_{\mathrm{r}1}$ and $m_{\mathrm{r}4} = m_{\mathrm{r}2}$ and—provided that the four-velocity of each shell is continuous at the location of collision—the momentum conservation can be shown to be equivalent to the relations [36]

$$p_3 = p_1 + \Delta p\,, \tag{3.1}$$

$$p_4 = p_2 + \Delta p\,, \tag{3.2}$$

where $p_i = m_{\mathrm{r}i}(\mathrm{d}r/\mathrm{d}\tau)_i$ stands for the 3-momenta of ith shell—here the indexing of the shells follows the notation applied on the left hand side of Fig. 3—and

$$\Delta p = -\frac{m_{\mathrm{r}1}m_{\mathrm{r}2}}{r_{\mathrm{c}}}u_1^a n_{2a} = \frac{(m_{\mathrm{g}1} - h_1)\,p_2 - (m_{\mathrm{g}2} + h_2)\,p_1}{r_{\mathrm{c}} - 2(m_{\mathrm{c}1} + m_{\mathrm{g}1})}\,, \tag{3.3}$$

where r_{c} is the radius at the collision, $m_{\mathrm{r}i}$ and $m_{\mathrm{g}i}$ stand for the rest mass and the gravitational mass of ith shell, $m_{\mathrm{c}1}$ denotes the central mass, while u_i^a, n_i^a and $h_i = m_{\mathrm{r}i}^2/(2r_{\mathrm{c}})$ denote the four-velocity, the unite normal and the 'self-gravity' of the ith shell, respectively.

Note that in (3.1) and (3.2) **the** both of the positive signs in front of the term Δp are correct as, in order to suit to the three-momentum conservation, Δp itself is negative. The apparent conflict may be resolved immediately if one takes into account that p_3 and p_4, as well as p_1 and p_2 are components of four-momentum vectors with respect to different bases [36]. It also follows from $\Delta p < 0$ that in order to have a transparent collision **happens** the vector fields u_1^a and n_2^a have to be arranger such that the contraction $u_1^a n_{2a}$ be positive.

From the four-momentum conservation the 'energy ballance' relations

$$m_{\mathrm{g}3} = m_{\mathrm{g}1} - \Delta\mathcal{E}\,, \tag{3.4}$$

$$m_{\mathrm{g}4} = m_{\mathrm{g}2} + \Delta\mathcal{E}\,, \tag{3.5}$$

can also be derived, where $m_{\mathrm{g}1} = M_2 - M_1$, $m_{\mathrm{g}2} = M_3 - M_2$, $m_{\mathrm{g}3} = M_3 - M_4$, $m_{\mathrm{g}4} = M_4 - M_1$, the M_i stand for the mass parameter of the ith Schwarzschild region as indicated **by on** the left panel of Fig. 3 and the measure of the 'energy transfer', $\Delta\mathcal{E}$, can be given as

$$\Delta\mathcal{E} = -\frac{m_{\mathrm{r}1}m_{\mathrm{r}2}}{r_{\mathrm{c}}}u_1^a u_{2a}\,. \tag{3.6}$$

Since both u_1^a and u_2^a are future directed timelike vectors the contraction $u_1^a u_{2a}$ is negative implying that $\Delta\mathcal{E}$ is always positive. This, in particular, means that the outer shell lose energy meanwhile the energy of the inner shell becomes larger.

In Subsection 4.3 the above relations are going to be economized in **deriving an explanation of characterizing** the mass inflation phenomenon.

In the other, totally inelastic case, i.e. whenever the interaction between the particles forming the colliding shells is so strong that only a single outgoing shell comes out from the crossing of them—as it was discussed in details in the appendix of [8]—the conservation of the four-momentum leads to the relations

$$h_3 = h_1 - m_{\mathrm{g}2} - \frac{(m_{\mathrm{g}2} + h_2)(p_1^2 - m_{\mathrm{g}1}^2 + h_1^2) + 2\,p_1\,h_1\,p_2}{h_1^2\,f(r_{\mathrm{c}})}, \tag{3.7}$$

$$p_3 = p_1 - \frac{p_2\,(p_1^2 - m_{\mathrm{g}1}^2 + h_1^2) + 2\,p_1\,h_1(m_{\mathrm{g}2} + h_2)}{m_{\mathrm{g}1}^2\,f(r_{\mathrm{c}})}. \tag{3.8}$$

where $f(r)$ stands for the metric function $1 - 2(m_{\mathrm{c}1} + m_{\mathrm{g}1})/r$ of the region between the two shells in advance to the collision. Note that in practice $m_{\mathrm{r}3} = \sqrt{2r_{\mathrm{c}}h_3}$ and $v_3 = (\mathrm{d}r/\mathrm{d}\tau)|_{r_{\mathrm{c}}} = p_3/m_{\mathrm{r}3}$ can always be uniquely determined by making use of (3.7) and (3.8).

The validity of the above relations were checked in case of simultaneous collisions of three shells—both for totally inelastic and mixed type of collisions—and it was found that the result is independent of the order of the pairwise collision of the shells. Similar justification were yielded in the case of exclusively totally transparent collisions where virtually three shells were created by splitting one of the shells into two equal mass shells—these were assumed to be in rest with respect to each other—and the order of the pairwise collisions were varied.

Note that in case of multi-layer shell systems one should take into account the possibility of simultaneous collisions of more than two shells. Since the occurrence of these type of events practically is of zero measure by choosing the timesteps to be sufficiently small we could guarantee that in each time step merely pairwise collisions occurred. It is also importart to note that whenever a simultaneous collision of more then two sheels are allowed to happen the result may always be determined by decomposing the event into pairwise collisions and the result is independent of the order of the pairing process.

As it may be anticipated the corresponding basic relations in the Newtonian framework are much more simple. For instance, in the totally transparent case they reduce to $M_3 = M_1$ and $M_4 = M_2$, and $V_3 = V_1$ and $V_4 = V_2$, while in case of a totally inelastic collision they are given as $M_3 = M_1 + M_2$, and $V_3 = (M_1V_2 + M_2V_2)/M_3$.

Note, finally, that in the Newtonian case the basic equations for totally transparent collisions are simple as the masses and the velocities are interchanged in the most obvious way.

3.2. Dynamics of multi-layer shell systems

In describing the relative motion of multi-layer shell systems we need to specify a reference parameter. As far as considerations are restrected to two shells the most convenient reference parameter is the Schwarzschild time coordinate defined in the intermediate region while we remain in the region of outer communication, whereas

inside the black hole region the Eddington–Finkelstein null coordinate do the same job for us. Let us mention that without choosing an appropriate reference parameter one may create significant confusion even in the (simplest possible) case of **describing the relative motion of** two shells. For instance, in [37] where the respective proper times measured along the separate shells—these, in virtue of (2.24) and (2.25), may differ considerably—are supposed to coincide, and used as **playing the role of a** reference parameter **for both shells**, false conclusions **are were** derived concering, e.g., the extent of regions where the crossing of **the** shells may occur.

In describing the motion of multi-layer systems consisting of $N\,(>2)$ shells, labeled by the index $i\in\{1,...,N\}$, the Schwarzschild time coordinates defined in the respective intermediate regions, associated with any pair of shells next to each other, is—as far as only the two shells are concerned—as suitable as before♯. However, as it was discussed before, these Schwarzschild time coordinates cannot be matched properly due to their discontinuities across the shells. To overbridge this technical difficulty the following synchronization process may be applied. In each of the intermediate regions the $t=const$ **the constant** t**-**lines determine simultaneity. The entire spacetime–built up from piecewise Schwarzschild regions—gets to be synchronized by applying to succeeding intermediate regions this synchronization process starting from the innermost region.

By making use of this synchronization method the location, i.e. the $r^{(i)}$ coordinates of all the shells can be given as a function of the time coordinate of the innermost region, playing the role of reference parameter, t_r. On most of the following figures instead of plotting the $r^{(i)}(t_r)$ functions the expressions $\Delta r^{(i)}(t_r)=r^{(i)}(t_r)-\bar{r}(t_r)$, where $\bar{r}(t_r)$ denotes the **mean value radial center of mass** of the $r^{(i)}(t_r)$ **functions distribution**, i.e. $\bar{r}(t_r)=\sum_{i=1}^{N}r^{(i)}(t_r)/N$ $\bar{r}(t_r)=\sum_{i=1}^{N}m_{\rm r}^{(i)}r^{(i)}(t_r)/\sum_{i=1}^{N}m_{\rm r}^{(i)}$, will be plotted††. Interestingly, in certain cases**, e.g. in case of a collapsing shell system where** $\bar{r}=\bar{r}(t_r)$ **is guaranteed to be a monotonously decreasing function**, instead of t_r the **mean value radial center of mass** $\bar{r}$ can also be used as a reference parameter. For instance, on some of the figures (see, e.g., Figs. 4, 5 and 7) the functions $\Delta r^{(i)}=\Delta r^{(i)}(\bar{r})$ will be plotted.

It is important to keep in mind that the above defined synchronization have certain extent of ambiguity concerning the specific t_r-value at a given point. Nevertheless, once the synchronization is fixed even at the crossings of shells are well-defined as the t_r-labels are uniquely determined, i.e. the motion of the shells may be properly represented in the (t_r,r) local coordinates. Note also that using the Schwarzschild time coordinates in the intermediate regions we may follow the motion of the shells only up to the appearance of

♯ If the motion is wished to be described inside the event horizon in these intermediate regions Eddington–Finkelstein null coordinates have to be applied instead of the Schwarzschild time as it has been indicated several times. Note also that because of spherical symmetry we frequently replace the spacetime by its factor space with respect to the group SO(3).

††By simply reversing the orientation of the synchronization, i.e. by starting from the outside we may also use as our reference time the Schwarzschild time coordinate of the external region.

the event horizon in either of these regions. One could argue that an external observer cannot see what happens with the shells beyond an the event horizons which manifest themselves by infinite value of the Schwarzschild time coordinate. Nevertheless, in some cases such as in the study of mass inflation discussed in Subsection 4.3 it is important to descend **below the horizons into the black hole region**. Fortunately, just like in the case of a single shell, the use of the Eddington–Finkelstein null coordinates instead of the Schwarzschild time coordinates **provides a satisfactory resolution of this technical resolve the corresponding** problem of synchronization for multi-layer systems**, as well**.

3.3. Initial data for systems

In specifying the initial data for a shell system, just like in the simple shell case, we need as an environmental parameter the central (Schwarzschild) mass, $m_{\rm S}$, characterizing the innermost region. The rest of the initial data set consists of the triples $m_0^{(i)}$, $r_0^{(i)}$, $v_0^{(i)}$ for the individual shells, with $i \in \{1, 2, ..., N\}$, which **are required to** satisfy the relations $r_0^{(i)} < r_0^{(j)}$ for $i < j$. **Having these inequalities hold** In determining the gravitational mass, $m_{\rm g}^{(i)}$, of the ith shell—by making use of the pertinent form of (2.16)—we need to know the central mass, $m_{\rm c}^{(i)}$, felt by the ith shell. It can be **seen justified** that for $i > 2$ the relation $m_{\rm c}^{(i)} = m_{\rm c}^{(i-1)} + m_{\rm g}^{(i-1)}$ **is satisfied holds**, with **assuming that** $m_{\rm c}^{(1)} = m_{\rm S}$ **holds**. Note that the initial data $m_0^{(i)}$, $r_0^{(i)}$, $v_0^{(i)}$ have also to satisfy for each individual shell the pertinent form of (2.17). **and the value of the sign factors $\epsilon_g^{(i)}$ have to be determined by following the argument outlined in Subsection 2.3.**

Note that in specifying the initial state of our multi-layer shell system the EOS of the **separate individual** shells**, along with the type of their collisions if any happens,** have to be **chosen fixed**. **Moreover, if inelastic collisions occur the EOS of the new shell produced by the merger is also needed to be fixed.**

3.4. The numeric algorithm

A detailed documentation of the applied numerical algorithm can be found in [52], providing also a link to the web page where from The open source C++ code **of the applied numerical algorithm can be found at [52]. may also be downloaded.** This subsection is to provide a short outline of this numerical algorithm.

Apart from **shell collisions** the motion of **each the individual** shells can be treated separately whence we **drop suppress** the indices of shells **below hereafter**. In order to be able to integrate the equations of motion—see (2.11)—we need to know $m_{\rm c}$, $m_{\rm g}$ and $m_{\rm r}(r)$. Once $m_{\rm c}$ and suitable initial data—consisting of m_0, r_0 and v_0— are specified the value of $m_{\rm g}$ and $m_{\rm r}(r)$ can determine as on one hand $m_{\rm g}$ is given by (2.16) while, on the other hand, $m_{\rm r}(r) = 4\pi\sigma(r)r^2$ and the functional relation $\sigma = \sigma(r)$ can be deduced, with the help of an EOS, as it **iswas** described at the end of Subsection 2.1. For instance, in the particular case of a dust or fluid shell with a homogeneous linear

EOS $m_{\rm r}(r)$ can be given analytically by making use of (2.15). In all the other more generic cases numerical algorithms can always be used in solving (2.14).

Once $m_{\rm r}(r)$ is known the absolute value of $\mathrm{d}r/\mathrm{d}\tau$, along with $(\mathrm{d}t_{\pm}/\mathrm{d}\tau)$, can be determined as a function of the radius by making use of (2.11), (2.24) and (2.25). The sign in front of the velocity $\mathrm{d}r/\mathrm{d}\tau$ depends on the initial data and its value remains fixed **until the appearance of a turning point of the shell if it occurs at all up to the critical radius**. The velocity, with respect to the Schwarzschild times, $\mathrm{d}r/\mathrm{d}t_{\pm}$, can also be given by applying the chain rule

$$\frac{\mathrm{d}r}{\mathrm{d}t_{\pm}} = \frac{\mathrm{d}r}{\mathrm{d}\tau}\left(\frac{\mathrm{d}t_{\pm}}{\mathrm{d}\tau}\right)^{-1} . \tag{3.9}$$

In describing the motion of a multilayer shell system, proceeding from the inside to the outside, we need to apply the synchronization outlined above. Therefore the motion of each shell is determined with respect to both the inner and outer Schwarzschild time (or the Eddington–Finkelstein null coordinates) because—as it follows from the synchronization process—in specifying the 'time step' in the outer regions we need to know the 'time step' applied in the innermost region.

In integrating the equations of motion the fourth order Runge–Kutta algorithm was applied. The appearance of a turning point in the integration process is indicated by the fact that the right hand side of (2.11) became negative. When this happens the code step back one and by making use of a root finding the location of the turning point is determined. The equation of motion (2.11) is integrated then such that the sign of the velocity, $\mathrm{d}r/\mathrm{d}\tau$, calculated from it is changed to the opposite of its previous value. A change in the order of the shells, i.e. the ordering of their radial coordinates, always indicates that a collision happened somewhere. Then the evolution of the system was held on, for a short while, until the precise location (in space and time) of the collision was determined by linear approximation. At that event by making use of the conservations equations and the assumption about the EOS we determined the initial data for the new shell(s). (**In case of an If inelastic collisions are allowed to occur the number of shells has to be decreased by one.)** The evolution of the full multi-layer system is carried on with the inclusion of the yielded new shell(s) afterwards. Once the innermost shell reached the origin, the evolution of the system was continued such that it was taken out from the system of shells and its gravitational mass was added to the center mass of the innermost region. Whenever the Eddington–Finkelstein coordinates were applied the algorithm was basically the same with the distinction that derivatives $\mathrm{d}t_{\pm}/\mathrm{d}\tau$ were replaced with the corresponding expressions $\mathrm{d}v_{\pm}/\mathrm{d}\tau$.

The precision of the applied numerical schema is checked in case of a system formed by two repeatedly intersecting equal rest mass dust shells (see Fig. 11 in Section 4.3). It is justified there that the our numerical code is convergent even though succeeding collisions happen.

4. The main results

One of the most interesting questions in working with **the systems of** thin shells **framework is whether a shell of this type does really correspond, in an appropriate sense, to a is how closely the behavior of thick shells, yielded by idealization of bounded continuous matter distributions. thick shell model, possibly to an idealization of a continuum matter distribution.** However tempting **this expectation certain analogies** might be one should keep in mind that even though one is using a huge number of thin shells the continuum distributions cannot be properly modelled, with the exception of the dust case, because in the thin shell limit the interaction of particles in the direction transversal to the shells**, other then —apart from the gravitational one—is neglected**. What is possible to be done consistently is to **provide investigate** an approximate modell using **possibly** a large number of dust shells. Let us mention here that the only attempt to **make investigate** such an approximate model—as far as we know—was done in [50] although the number of the shells was kept to be minimal, i.e. only the evolution of a two-shell system was investigated there. As opposed to this with the help of our C++ code [52] **the evolution of a** large number of shells can be **evolved determined**. **Nevertheless, for a clear separation of the various effects and to get used to the applied framework, in the first part of this subsection, each multi-layer system—with one exception—will consist of 16 shells. In order to make the significance of the change of certain parameters to be transparent on the following graphs the initial parameters or conditions will always be changed one by one.**

4.1. The study of 'simple' systems

In order to provide a better understanding of the dynamics of our thick shell mimicking multi-layer thin shell system as reference solutions first the evolution of $N = 16$ shells with uniform initial mass and radial distributions will be examined. Since even in this case there are too many parameters characterizing the the system it seems to be appropriate—and actually this will be done below—to proceed in small steps by changing the initial conditions of the reference solution almost parameter by parameter.

As mentioned above we shall consider the time evolution of shell systems consisting of $N = 16$ shells, with the exception of panel (c) in Fig. 4 where the evolution of $N = 64$ shells will be considered. The total rest mass $\sum_{i=1}^{N} m_0^{(i)}$ of these shells will be 72, while $m_S = 0$, in each of the following cases. The mass distribution will be uniform on each panels of Fig. 4, while it is uniform on panel (e) and centered on panel (f), possessing mass distribution as specified by (4.1). The initial radial distribution $r_0^{(i)}$, in case of uniform distributions are chosen so that $r_0^{(i)} = 1999 + i$, where i runs from 1 to 16. It is centered on panel (f) and it is random on panels (g) and (h) in Fig. 5. It is important to keep in mind that even in case of a uniform mass distribution only the rest masses $m_0^{(i)}$

could be arranged to be equal to each other, whereas the corresponding surface mass densities $\sigma_0^{(i)}$ differ slightly according to the relations $m_0^{(i)} = 4\pi\sigma_0^{(i)} {r_0}^{(i)}$. For simplicity, only dust shells are considered—with the exception of panel (d) in Fig. 4—and the initial velocity, $v_0^{(i)}$, of them were chosen to be zero, i.e. all the shells start from rest.

On each of the panels of Figs. 4 and 5 on the horizontal axis the **mean value radial center of mass** $\bar{r}$ is indicated, which, in particular, means that the synchronized events are arranged so that they lie along vertical segments. The initial radius distribution of the shells are indicated by strokes on the right side of each plot. In order to help the recognition of the **main characters of the evolutions developing structures** the following type of gray shadowing had been applied. A lighter gray shadow was used beetween the momentary outermost and the last but one shells while the complementary inner part received a bit darker gray coloring. Since we intended to compare the Newtonian and fully relativistic time evolutions in the relativistic case all the plots were produced by making use of the Schwarzschild time cooordinates, whence all the evolution stops before reaching 'the even horizon'.

Let us provide now a brief outline of the plots in Figs. 4 and 5. The letters applied in the following itemization refer to the labels added to the individual panels.

(a) In the Newtonian setup the time evolution of the above specified shell system with uniform radius and mass distribution is shown.

(b) The time evolution, with initial data corresponding to that of panel (a), is depicted in the fully relativistic case.

(c) It is to justify that the basic characters do not change drasticly whenever the numbers of the shells is increased **by a factor of four**. The time evolution of 64 shells is depicted in the fully relativistic case.

(d) The fully relativistic time evolution of 16 shells is considered using the same initial configuration as on panel (b) with the distinction that the EOS of the shells is homogeneous linear, $\mathcal{P} = w\sigma$ with $w = 0.006$. °

(e) On this plot **those differences are intended to be shown which characterize** the evolution of a**n initial data specification for which the distribution of positions is kept to be system with a** uniform **initial radial** but with the centralized **symmetric**

$$m_{\mathrm{r}}^{(i)} = \begin{cases} i, & \text{if } 1 \le i \le 8; \\ 16 - i, & \text{if } 9 \le i \le 16\,. \end{cases} \tag{4.1}$$

mass distribution is shown. **The latter is indicated by the thickness of the horizontal strokes at the right edge of each of the individual figures.**

(f) On this panel the **time** evolution of **shells a system,** with uniform **initial** mass distribution and with **symmetricly centered** radial distribution, is shown, where

° The order of magnitude of the value of w **presumes that the pressure is determined in was determined as if the shell system formed** a virialized system in the kinetic gas theory.

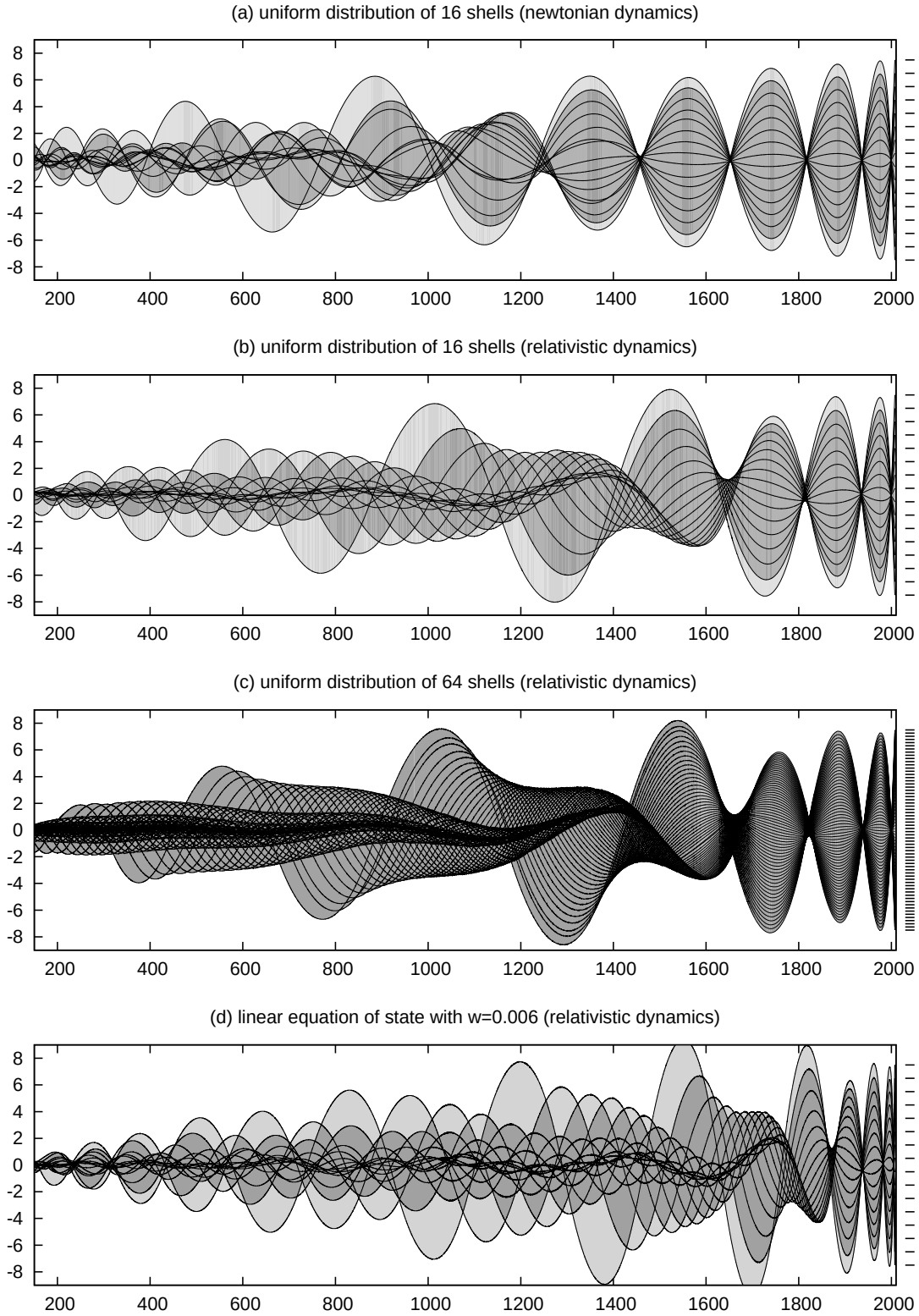

Figure 4. The time evolution of shell systems with uniform mass and initial radial distributions are shown. On the horizontal axis the **mean value radial center of mass**, $\bar{r}$, of radius of the shell system is indicated, while on the vertical axis the deviation $\Delta r^{(i)} = r^{(i)} - \bar{r}$ relevant for the individual shells are plotted. The upper two panels are to indicate the similarities and differences between the Newtonian and fully relativistic evolutions. **Although it might look strange first but it is important to keep in mind that for the depicted collapsing systems—where $\bar{r}$ is monotonously decreasing—here, and in Figs. 5, 7, 8, 9 and 10, time progresses from right to left.**

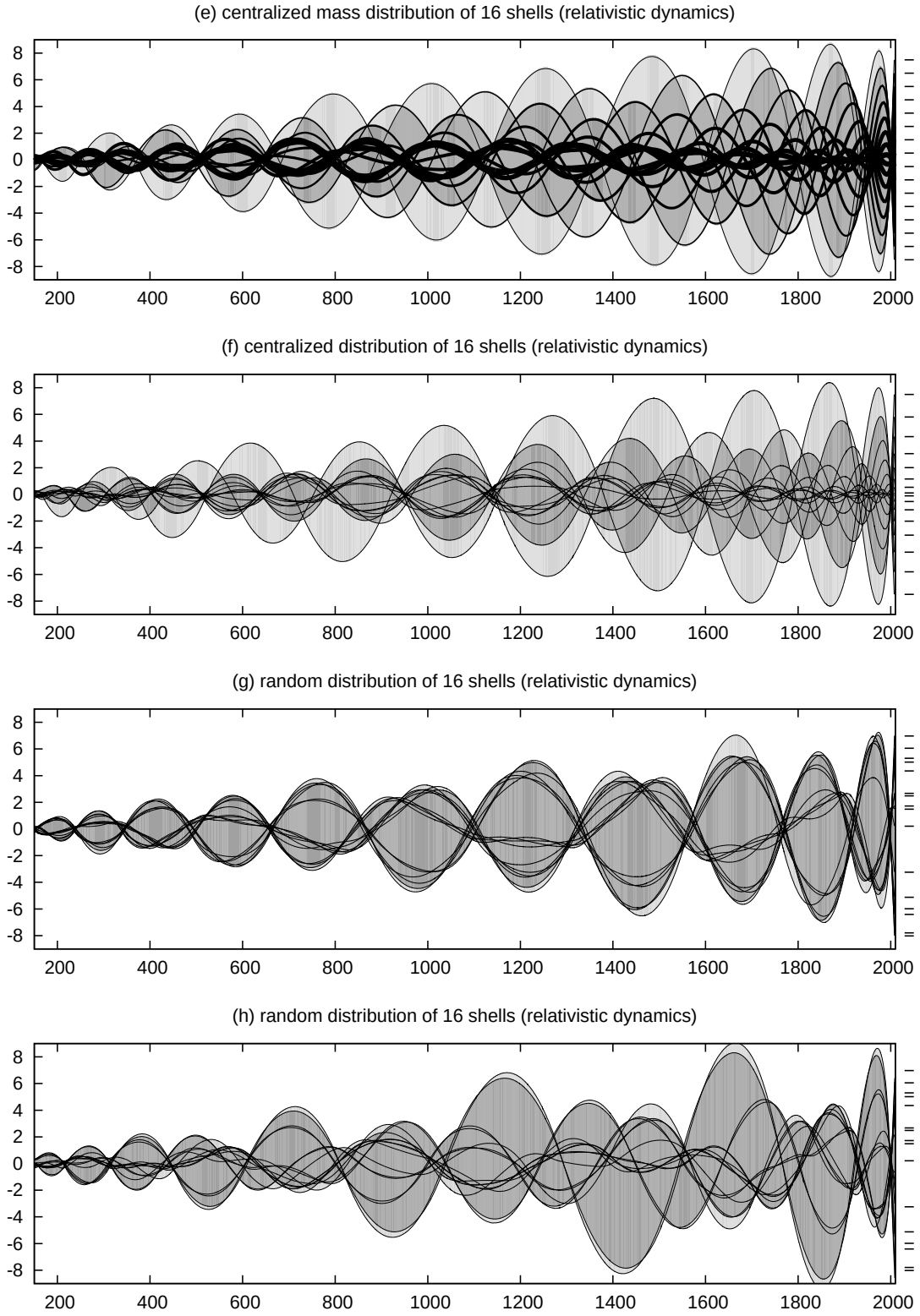

Figure 5. The time evolution of shell systems are shown. On the top panel the mass distribution while on the other three panels the initial radial distribution is non-uniform, in fact, the initial radial distribution is chosen to be random on the lower two panels. As in Fig. 4 on the horizontal axis the **mean value radial center of mass**, $\bar{r}$, of radius of the shell system is indicated, while on the vertical axis the deviation $\Delta r^{(i)} = r^{(i)} - \bar{r}$ relevant for the individual shells are plotted. In spite of the significant differences in the initial part of the indicated evolutions the similarities in the final parts is considerable.

$r_0^{(1)} = 2000$, $r_0^{(16)} = 2015$ and

$$r_0^{(i+1)} - r_0^{(i)} = (9-i)\cdot\Delta\,, \quad \text{for} \quad \mathrm{i} = 1,2,...,7\,; \tag{4.2}$$

$$r_0^{(i)} - r_0^{(i-1)} = (i-8)\cdot\Delta\,, \quad \text{for} \quad \mathrm{i} = 10,11,...,16\,, \tag{4.3}$$

with $\Delta = 15/71$.

(g),(h) On these two panels the mass distribution is uniform while the initial radial distributions are random although the initial location of the outermost shells were chosen to be the same as on all the other plots **by specifying, i.e.,** $r_0^{(1)} = 2000$ and $r_0^{(16)} = 2015$.

By comparing the plots in Figs. 4 and 5 the following conclusions may be drawn. It is clearly visible **in Figs. 4 and 5** that **in case of multi-layer shell systems,** whenever the shells are starting from rest not only the nearby shells cross but the crossing**s** of **all** the shells **tend to be accumulated seems to be generic**. It has been justified by our numerical experiences–see also panel (c) in Fig. 4—that **the developing basic structures seems to be** independent of the number of the shells. **this type of accumulations remained, i.e. they cannot be washed out this way.** Let us mention that shell crossings are known to occur even in the continuous modell of spherical dust systems [63]. Note, however, that they are also **frequently** referred **there** as 'shell crossing singularities'. **and although** This type of singularities are **not as strong as known to be much weaker than** the central ones**, newertheless,** in the continuous modell the evolution stops whenever they occur.

Returning to the interpretation of panels (a)-(d) of Fig. 4, and (g)-(h) of Fig. 5 by comparing these plots it is straightforward to recognize that either type of deviation from the uniform distribution yield a visible dispersion of the shells. The focusing of the shells is lost faster and the spreading is more intensive as the initial distributions get further and further away from uniformity.

Let us now make some more specific comments. Comparing panels (a) and (b), depicting the Newtonian and relativistic evolution of completely uniform distributions it is visible that the non-linearity of the relativistic evolution yield larger dispersion indicated by the fact that in the Newtonian case the first five knots are pretty well-focused while the loss of the coherence starts earlier in the relativistic case. Panels (c) and (d) of Fig. 4 justify that the main characters of the evolution do not change whenever either the number of the shells are increased or the EOS is changed a little bit. On panel (e), where the initial mass distribution is centered, as it is specified by (4.1), knots do not develop and at the beginning the dispersion of the system dominates. On the other hand, during the second half of the **evolution indicated period** the shells start to be concentrated around two of the highest mass shells, and then the groups formed this way start to oscillate around each other. On panel (f), where instead of the mass distribution the initial radial distribution is concentrated, a similar pair of groups of shells can be seen to develop. On both panels (e) and (f) it is also visible that the **motion radius** of the outermost shell vary on a significantly larger scale than on the

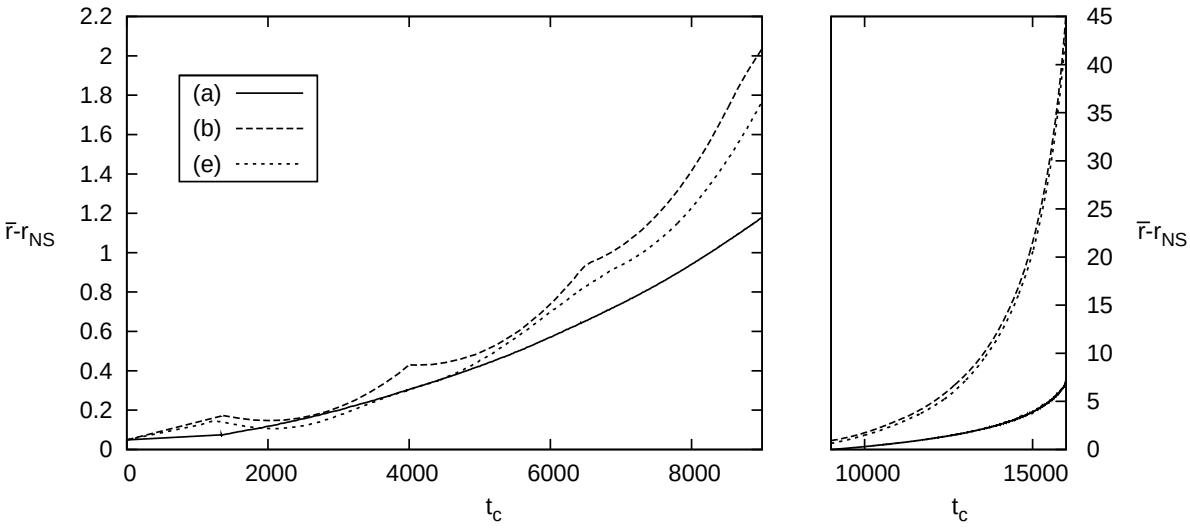

Figure 6. The time dependence of **average of the radius of the differences of the radial center of mass values of** the shell systems depicted on panels (a), (b) and (e) in Figs. 4 and 5 **and that of Newtonian reference solution of a single shell with mass** $M_{\rm shell} = 16$ is indicated by plotting the $\bar{r} = \bar{r}(t_{\rm c})$ $\bar{r}(t_{\rm c}) - r_{\rm NS}(t_{\rm c})$ functions, where $t_{\rm c}$ denotes the Minkowski time in the central region. $\bar{r}(t_{\rm c} = 0) = 2007.5$ **and** $\bar{r} - r_{\rm NS} = 0$ **at** $t_{\rm c} = 0$ **for each of the individual systems. For the sake of curiosity the evolution of a shell which would have been yielded by the inelastic collision of all the shells in configuration (b) is also represented by the dotted line (i).**

other panels. In particular, their oscillation amplitude increase during the **first period initial part** and start to decrease only later. Nevertheless, the relative variety on their motion, with respect to the characteristic size of the shells composed by all but the outermost, remains significant during the entire evolution. The gray shadowing makes this type of effects to be more transparent. On panels (g) and (h) the initial **part the** distribution of the shells is random. **inside the boundary which is chosen to be the same as they were for all the configurations depicted by Figs. 4 and 5.** It is clearly visible on **these** panels **(g) and (h)** that although **at the beginning phase there is an apparent chaotic behavior of the shells which, however, latter ends up the development of knots and during the initial part the behaviors appears to be chaotic in the later period patterns, i.e.** similar grouppings of the shells **observed develop** as **it happened** in case of the other systems.

In order to make the differences of the above discussed dynamics to be more amenable, in Fig. 6, the **time** dependence of **the differences,** $\bar{r} - r_{\rm NS}$ **of the mean value radial center of mass**, $\bar{r}$, **of the radius** of the shell system depicted on panels (a), (b) and (e) in Figs. 4 and 5 **on the Minkowski time,** $t_{\rm c}$**, of the central region** is shown, **where** $t_{\rm c}$ **denotes the Minkowski time of the central region and** $r_{\rm NS} = r_{\rm NS}(t_{\rm c})$ **stands for time dependence of the Newtonian reference**

solution of a single shell with mass $M_{\rm shell} = 16$. On the left panel of Fig. 6 a zoom to the **beginning final** part of the evolution is shown in order to make the **slight** differences more visible. Note that the wavy figures do correspond to the formation knots indicated by the initial parts of the time evolution on panels (b) and (e) of Figs. 4 and 5. **It is worth to be emphasized that the radial center of mass,** $\bar{r} = \bar{r}(t_{\rm c})$**, is a monotonously decreasing function for each of the individual systems.**

4.2. Dispersion of small perturbations

In this subsection the number of shells is increased significantly from N=16 to **either 91, 100 or** 101 **in our reference simulation with uniform initial mass and radial distributions shown by the upper left panel of Fig. 7. In order to make the figures to be more accessible the shells will be arranged to be of equal rest mass, all of them starts from rest and only the initial radial distribution is perturbed slightly. Note that according to our experience—supported by comparison of panels (e) and (f) in Fig. 5—we do not expect that perturbation in the mass distribution, while keeping the radial distribution uniform, would yield significantly different evolution from the evolution corresponding to a similar perturbation in the initial radial distribution while keeping the mass distribution uniform. Therefore only the latter type of perturbations will be considered below.**

The **applied** small perturbations on the evolution of equal mass shell systems are produced either by doubling the mass of a single shell (or ten shells) of **a formerly an initially** uniform distribution, or by taking out a single shell (or ten shells) from **a formerly an initially** uniform distribution. The initial part of **the** evolutions of these slightly perturbed systems are compared to that of an initially uniform distribution**, the latter is shown by the upper left panel of on** Fig. 7.

The evolutions relevant for systems where the rest mass of one or **nine ten** shells is doubled are shown on the upper middle and upper right panels. The change of the motion of the other shells is noticeable but **for the first glance** it is not too striking. As opposed to this, on the panels on the **central line lower row** of Fig. 7**—where on the left and middle panels only a single shell is removed, while ten shells are taken out from the initially uniform distribution on the right panel—** the **slight** perturbations yield more significant changes. **In particular, on the central left and bottom middle panels only a single shell is removed, while nine shells are taken out from the initially uniform distribution on the central right panel.** The **effect consequences** of **these the indicated small** changes **is are** more **transparent significant** in spite of the fact that the change of the total rest mass is about 1%**, e.g.,** whenever only **one single** shell is left out from the **reference simulation with** uniform **initial** distributions.

By the inspection of the figure above the following important qualitative observations can be made. First of all, there is a tendency of the formation of

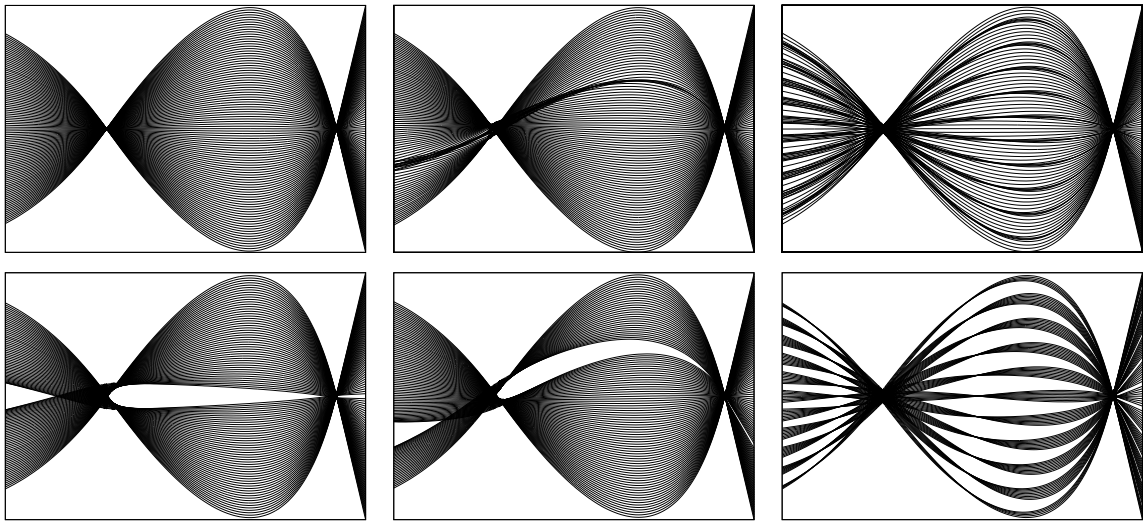

Figure 7. The initial part of the evolution of slightly perturbed initially almost uniformly distributed multi-shell systems possessing 'anti-gaps' and gaps consisting of about 100 shells, are shown. On the horizontal axis the mean value of the radius of the shell system, $\bar{r}$—which takes values from the interval $[9425, 10050]$—, while on the vertical direction the deviations, $\Delta r^{(i)} = r^{(i)} - \bar{r}$, are indicated. On the plot at the *upper left* corner $r_0^{(i)}$ are chosen such that they are symmetric to $r_0^{(51)}$ with $r_0^{(i)} = 9999 + i$, while $m_0^{(i)} = 1$ for $i = 1, 2, ..., 101$. On these plots the initial parts of the evolution of shell systems yielded by slight perturbations of a reference system—consisting of 101 uniformly distributed equal mass shells starting from rest, depicted by the *upper left* panel—are shown. The initial radial distribution, $r_0^{(i)}$, of the reference system is chosen such that the location of the shells is symmetric to $r_0^{(51)}$ with $r_0^{(i)} = 9999 + i$, while $m_0^{(i)} = 1$ and $v_0^{(i)} = 0$ for $i = 1, 2, ..., 101$. The systems with 'gaps' shown on the *lower left* and *lower middle* panels are resulted by removing the 51th and 31th shells from the reference system, respectively. The *upper middle* panel shows a system with an 'anti-gap' where the mass of the 31th shell is doubled, i.e. $m_0^{(31)} = 2$. On the *right panels* the evolution of systems with 10 uniformly distributed gaps or anti-gaps are shown. The radial center of mass $\bar{r}$ is indicated on the horizontal axis—which takes values from the interval $[9425, 10050]$ on each panel—, while on the vertical direction the deviations, $\Delta r^{(i)} = r^{(i)} - \bar{r}$, are shown.

a 'crust'—represented by the increase of the density of shells—at the edges of the widening gaps. Second, following the widening of a gap a reversing of the sides also occur, i.e., the innermost shell gets to be the outermost and vice versa, as it is clearly visible on the colored figure. In addition, the crusts are growing ant the two crusts starts to move as if the entire system gradually became a two-shell system. Third, around the anti-gaps an increase in the density of shells is also noticeable although the growing rate is much less than in case of gaps. The two right panels on the first and second lines in Fig. 8 indicate that the evolution of systems with gaps

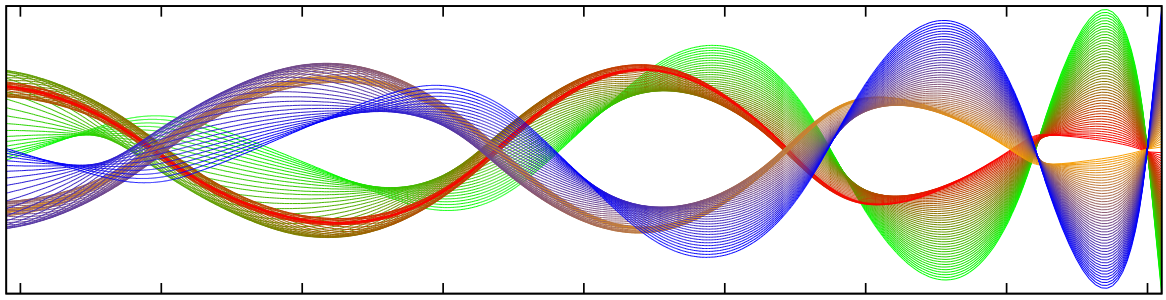

Figure 8. On this colored plot a longer period of the time evolution, for the system on the *lower left* panel of Fig. 7, is shown. It demonstrates that a slight change of the uniform initial data might result significant differences in the long run and formation of 'crusts' and reversing of sides are also noticeable.

and anti-gaps gets closer to each other when a large number of gaps and anti-gaps are uniformly distributed in the initial configurations.

4.3. Mass inflation

In starting this subsection we would like to mention that some of the arguments below were motivated by claims of [36] about the time evolution of a system formed by a pair of repeatedly intersecting equal rest mass shells. However, we would like to emphasize that our conclusions about the possible rate of the blowing up of the mass of the intermediate regions—these are also justified by means of numerical investigations **below**—differs from that of [36].

In describing the unbounded growth of mass recall first that the squares of energy and momentum exchanges, $\Delta\mathcal{E}$ and Δp,—for their definitions see Subsections 3.1—are related as

$$\Delta\mathcal{E}^2 - \Delta p^2 = \frac{{m_{\mathrm{r}1}}^2 {m_{\mathrm{r}2}}^2}{{r_{\mathrm{c}}}^2} \tag{4.4}$$

which implies that for $\Delta\mathcal{E}$ the inequality

$$\Delta\mathcal{E} \geq \frac{m_{\mathrm{r}1} m_{\mathrm{r}2}}{r_{\mathrm{c}}} \tag{4.5}$$

holds. Now, by making use of the relations $m_{\mathrm{g}2} = M_3 - M_2$ and $m_{\mathrm{g}4} = M_4 - M_1$, along with the vanishing of $m_{\mathrm{c}1} = M_1$, in virtue of (3.5), we get that

$$M_4 + M_2 = M_3 + \Delta\mathcal{E}\,. \tag{4.6}$$

Hence, in virtue of (4.5) and (4.6), for the **mean value radial center of mass**, $\overline{M} = (M_4 + M_2)/2$, of the mass parameters of the **succeeding successive** intermediate regions the relation

$$\overline{M} \gtrapprox \frac{1}{2}\left(M_3 + \frac{m_{\mathrm{r}1} m_{\mathrm{r}2}}{r_{\mathrm{c}}}\right) \tag{4.7}$$

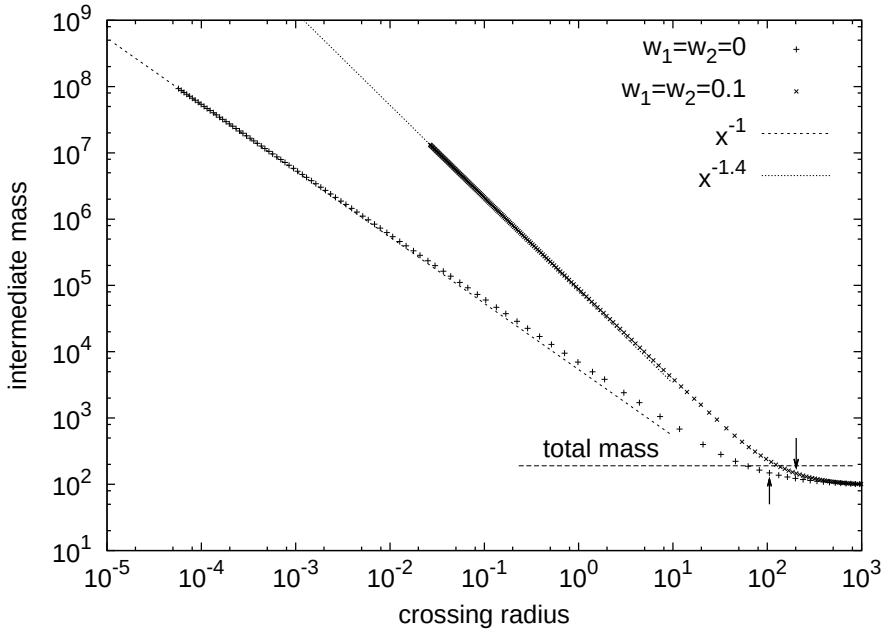

Figure 9. The *log-log* plot of the mass parameter of the intermediate region with respect to the radial coordinate of the collisions is shown for a system formed by two repeatedly intersecting equal rest mass shells possessing linear EOS with w_1 and w_2. Note that the dots on this figure signify at the location of the collision the value of the mass of the intermediate region produced in the collision, while between any two collisions the mass of the intermediate region is constant. The plot with $w_1 = w_2 = 0$ corresponds to the case of colliding dust shells. In both cases the initial data was synchronized in the Schwarzschild time of the intermediate region and it was chosen to be the same as in [50], i.e. such that $m_{\mathrm{S}} = 0$, $m_0^{(1)} = 100$, ${m_{\mathrm{g}}}^{(1)} = 100$, $m_0^{(2)} = 100$, ${m_{\mathrm{g}}}^{(2)} = 90.05906$. **and** $v_0^{(1)} = v_0^{(2)} = 0$ **(Note that in virtue of (2.16)** ${m_{\mathrm{g}}}^{(1)}$ **and** ${m_{\mathrm{g}}}^{(2)}$ **determines the initial values** $v_0^{(1)}$ **and** $v_0^{(2)}$**.)** The low radius behavior of the plotted curves justify that the Schwarzschild mass of the intermediate regions grows as $\overline{M} \sim r^{-\alpha}$, where for α the fits to the estimate $\alpha = 1 + 2w_1 + 2w_2$ formulated by (4.8). The arrows point to the locations where the critical radiuses of the external region gets to be larger than the radiuses of the succeeding collisions, i.e. where ϵ_{t_+} for the outer shells change their sign, respectively.

has to hold. This latter inequality, whenever r_{c} tends to zero and $\Delta\mathcal{E}$ becomes much larger than M_3—for the case of colliding shells possessing linear EOS with $w_1 = c_{\mathrm{s}1}^2$ and $w_2 = c_{\mathrm{s}2}^2$—implies that $\overline{M}$ **must** tend to infinity **by following such that** the asymptotic blow up rule

$$\overline{M} \gtrapprox C r^{-(1+2w_1+2w_2)} \tag{4.8}$$

holds.

The process, which in repeated collisions of a pair of shells leads to an unbounded growth of the mass parameter of the intermediate region, is the mass inflation. **phenomenon** The **manifestation of the** blow up behavior**, relevant for of** some simple configurations, **justifying the correctness of along with the justification of** the estimate (4.8), is shown in Fig 9.

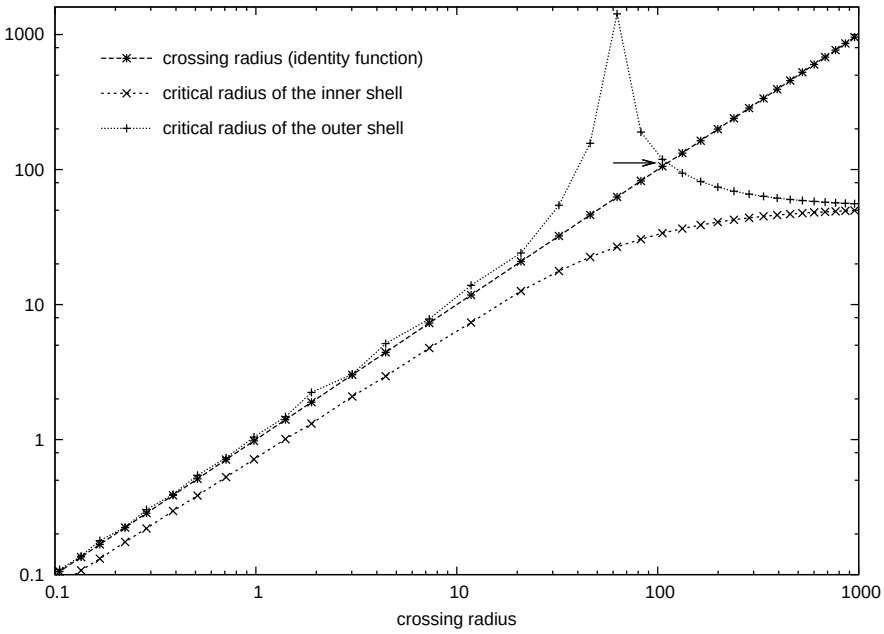

Figure 10. The values of $\widehat{r}_{\rm inner}$ and $\widehat{r}_{\rm outer}$ as a function of $r_{\rm c}$ are plotted on a *log-log* scale for the case of repeatedly colliding equal rest mass dust shells corresponding to the 'points' represented by the '+' signs in Fig 9. The intersection of the $r_{\rm c} = \widehat{r}_{\rm outer}(r_{\rm c})$ curves signifies—indicated by the arrow—the location where ϵ_{t_+} of the outer shell changes sign. Note also that gravitational mass of the outer shell changes sign where $\widehat{r}_{\rm outer}$ attains its maximum.

There are some remarks in order. In explaining the **apparently relatively** small values of w it should be mentioned that whenever **the larger** values of w_1 and w_2 is **larger (say it is about** 0.1**) applied,** or w_1 and w_2 differ significantly, the fluid shells start to move outwards and**/or it may happen that** they collide only once or they do not collide at all. It is also important to note that whenever the collapse and mass inflation occur the blow up rate behavior is insensitive to the **particular values of the** initial **data radiuses and velocities** of the shells.

Note that the mass inflation **phenomenon** is **not new, it is** known to occur in the continuum limit (see, e.g, [64] for **its detailed and a** recent numerical investigation). Nevertheless, for the first sight the occurrence of the mass inflation in the thin shell formalism is **surprising unexpected** because it is known that the mass of the intermediate region cannot be larger than that of the outer region unless the radius of the collision, $r_{\rm c}$, gets to be smaller than the critical radius, $\widehat{r}$ of the outer shell. Note that such a critical value in case of the dynamics of a single shell is extremely small, **far below much smaller than** the Schwarzschild radius. In order to show that the above formulated expectation is justified by the investigated time evolutions in Fig 10 the time dependentness of the critical radiuses of the inner and outer shells—their relative location varies in time—, along with the time dependence of the radius of the collision is plotted. The location where for the first time $r_{\rm c}$ gets to be smaller than $\widehat{r}$ for the temporarily outer shell is the very location where the mass of the intermediate region,

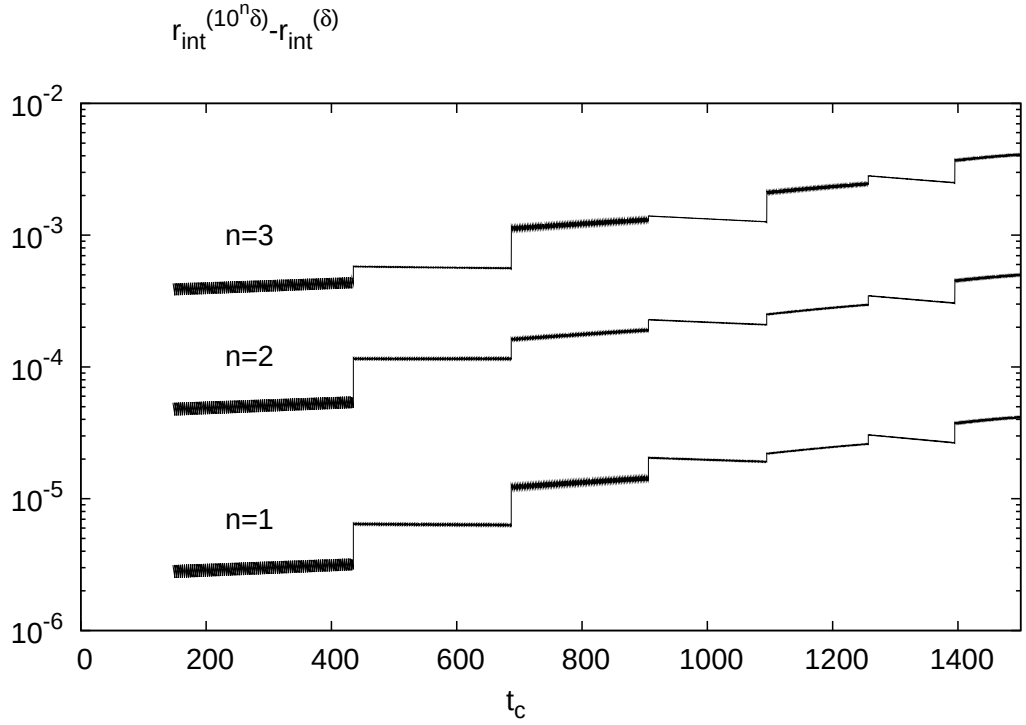

Figure 11. The time dependence of the difference, $r_{\rm int}^{(10^n\delta)} - r_{\rm int}^{(\delta)}$, of the numerical value of the radius of the (temporarily) internal shell is plotted relevant for resolutions $10^n\delta$ with $n = 1, 2, 3$ and for the reference numerical solution $r_{\rm int}^{(\delta)}$.

M_4, gets to be larger than the mass of the outer spacetime, M_3.

The precision of the applied numerical schema is determined in case of the above described system formed by two repeatedly intersecting equal rest mass dust shells. Denote by $r_{\rm int}^{(\Delta)}$ the numerical value of the radius of the (temporarily) internal shell relevant for resolution Δ. In Fig. 11 the time dependence of the difference $r_{\rm int}^{(10^n\delta)} - r_{\rm int}^{(\delta)}$ is plotted for the initial period for $\Delta = 10^n\delta$ with $n = 1, 2, 3$ and $r_{\rm int}^{(\delta)}$ denotes the reference numerical solution with smallest resolution δ. As it is expected for any fixed value of n the difference $r_{\rm int}^{(10^n\delta)} - r_{\rm int}^{(\delta)}$ is increasing in time, however, by decreasing the value of n by one yields an order of magnitude downward shift of the successive curves. This justifies that the our numerical code is convergent even though collisions—indicated by the jumps on the curves—happen.

Let us finally mention that mass inflation is not specific only for two-shell systems as it did also occur for systems consiting more than two shells. According to our experiences the masses of each of the intermediate regions increase following apparently the above derived power law rule but there was a definite order kept during the evolution. More definitely, at any instant of the Eddington–Finkelstein time the mass of an inner intermediate region

was in all of our simulations smaller than the mass of any of the intermediate regions located outwards with respect to the inner one.

5. Final remarks

The relativistic time evolution of multi-layer spherically symmetric shell systems has been investigated. After recalling the basics **and providing a critical review** of the analytic setup a newly developed numerical code is introduced. **and applied in various dynamical cases. Our This** numerical method was made to be capable to follow the time evolution of systems comprised by great numbers of colliding shells**, where the such that whenever** collisions **happen were assumed to be either they are assumed to be totally** transparent. **or inelastic**

A detailed investigation of the dynamics of numerous shell systems involving large number of shells was also presented. Our observations provide important clue in understanding the dispersion and the formation of groups of shells characterizing the dynamics of shell systems when their initial radial or mass distributions are non-uniform.

By making use of our numerical method for the first time the relativistic time evolution of numerous shell systems involving large number thin shells could have been made. As these systems may be considered as approximate models of thick shells the results reported in this paper provide insights about their dynamical behavior, as well. The most important observations we have made can be characterized by the key phrases: concentrations of subsets of shells, formation of 'crusts' at the boundaries, reversing of the sides of gaps.

It is also guaranteed by The chosen analytic setup **ensured** that the **dynamics evolution** of the considered shell systems can be investigated **everywhere, i.e.** both in the domain of outer communication and in the black hole region. **until the central singularity is reached by the shells** This **latter property** made our numerical code to be **suitable capable** to **investigate the demonstrate that** mass inflation **phenomenon occur** within the thin shell formalism. We would like to emphasize that beside the numerical investigation of mass inflation an estimate explaining the main features of the blow up behavior of the mass parameter of the intermediate region is also provided.

In closing this paper let us mention that there are several further applications of the developed analytic and numerical framework which, however, cannot be subject of the present paper. As an immediate example let us mention that the thin shell formalism can be used to investigate the critical phenomenon. In order to flash lights on the ideas beyond let us consider here the interaction of a system of dust shells, the individual members of which are moving outwards, and a low mass fluid shell, the initial data of which is chosen such that without the presence of the dust

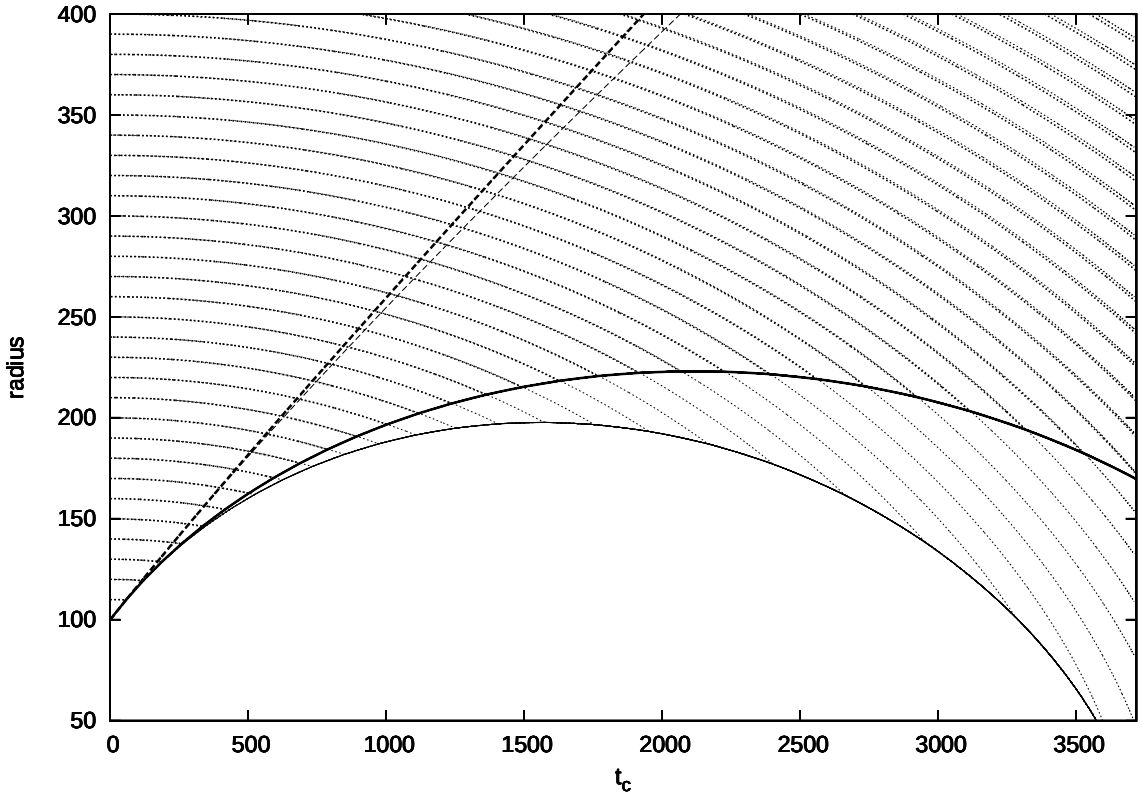

Figure 12. The time evolution of a system composed by a fluid shell and freely falling dust shells is shown in the fully relativistic (thick lines) and in the Newtonian case (thin lines). In both cases the fluid shell starts to move outwards either freely (dashed lines) or succeedingly colliding with the indicated sequence of dust shells (the latter start to move from rest and they are represented by dotted lines). In the fully relativistic case t_c stands for the Minkowski time of the central region, while it denotes the 'absolute time' in the Newtonian case. The initial data—$m_0^{\rm fluid} = 1$, $m_{\rm g}^{\rm fluid} = 1.01$, $m_0^{\rm dust} = 0.1$, $w^{\rm fluid} = 0.001$—is arranged such that in the non-interacting cases the radius of the fluid shell tends to infinity while in the case of inelastic collisions the fluid shell do collapse and a black hole develops or, in the Newtonian case, a point mass appears at the center.

shells it would expand forever reaching timelike infinity in the asymptotic limit. Both the motion of the free fluid shell and that of the interacting one are plotted on the left panel of Fig 12. For the sake of comparison, on the right panel of Fig 12 the corresponding Newtonian motion is also shown. As it can be seen, in both cases the fluid shell slowed down by the inelastic collisions with some of the dust shells and simultaneously its mass is increasing which leads to the formation of a turning point in its motion. In turn, the fluid shell collapses and the evolution ends up with the formation of a black hole, or a point mass appears in the Newtonian case.

Based on the above mentioned ideas we expect that by replacing the

dust shells with low mass prefect fluid shells with suitable EOS and by fine tuning the mass parameter or the initial velocity of innermost fluid shell one gets a system appropriate for the investigation of critical phenomenon within the thin shell formalism.

Let us finally mention that by replacing the innermost fluid shell in the above outlined investigations by a null shell one may also get a viable model of the interaction of the ejected radiation with the surrounding matter.

As it was mentioned in the introduction there is a great number of astrophysical systems which can be modelled by shells. For instance, the interaction of repeated quasi-spherical matter ejections by supernovas are planned to be investigated by the developed method.

Acknowledgments

This research was supported in part by OTKA grant K67942.

References

[1] López C A 1988 Dynamics of charged bubbles in general relativity and models of particles *Phys. Rev.* D **38** 3662
[2] Zloshchastiev K G 1999 Extended particle models based on hollow singular hypersurfaces in general relativity: classical and quantum aspects of charged textures *Int. J. Mod. Phys.* D **8** 165
[3] Varela V 2007 Neutral perfect fluids and charged thin shells with electromagnetic mass in general relativity *Gen. Rel. Grav.* **39** 267
[4] Corichi A *et al* 2006 Quantum collapse of a small dust shell *Phys. Rev.* D **65** 064006
[5] Ortíz L and Ryan M P Jr 2007 The complete quantum collapse scenario of a 2 + 1 dust shell: Preliminary calculations *J. Phys.: Conf. Ser.* **68** 012047
[6] Zloshchastiev K G 1999 Singular shells of quark-gluon matter *Int. J. Mod. Phys.* D **8** 363
[7] Ruffini R and Vitagliano L 2003 Energy extraction from gravitational collapse to static black holes *Int. J. Mod. Phys.* D **12** 121
[8] Gáspár M E and Rácz I 2010 Probing the stability of gravastars by dropping dust shells onto them *Class. Quantum Grav.* **27** 185004
[9] Ostriker J P and Gunn J E 1971 Do pulsars make supernovae? *Astrophys. J.* **164** L95
[10] Zaninetti L 2010 A law of motion for spherical shells in special relativity *Adv. Studies Theor. Phys.* **4** 525
[11] Hamity V H and Gleiser R J 1978 The relativistic dynamics of a thin spherically symmetric radiating shell in the presence of a central body *Astrophys. Space Sci.* **58** 353
[12] Koike T and Mishima T 1995 Analytic model with critical behavior in black hole formation *Phys. Rev.* D **51** 4045
[13] Visser M and Wiltshire D L 2004 Stable gravastars: an alternative to back holes? *Class. Quantum Grav.* **21** 1135
[14] Benedict M N Carter 2005 Stable gravastars with generalized exteriors *Class. Quantum Grav.* **22** 4551
[15] Visser M 1989 Traversable wormholes: Some simple examples *Phys. Rev.* D **39** 3182
[16] Visser M 1995 Lorentzian wormholes: from Einstein to Hawking, AIP Press, New York
[17] Poisson and Visser 1995 Thin-shell wormholes: Linearization stability *Phys. Rev.* D **52** 7318
[18] Lobo F S N and Crawford P 2004 Linearized stability analysis of thin-shell wormholes with a cosmological constant *Class. Quantum Grav.* **21** 391

[19] Eiroa E F and Romero G E 2004 Linearized stability of charged thin-shell wormholes it *Class. Quantum Grav.* **36** 651
[20] Dias G A S and Lemos J P S 2010 Thin-shell wormholes in d-dimensional general relativity: Solutions, properties, and stability arXiv:1008.3376v1
[21] Madea K and Sato H 1983 Expansion of a thin shell around a void in expanding Universe *Prog. Theor. Phys.* **70** 772
[22] Lake K and Pim R 1985 Development of voids in the thin-wall approximation. I – General characteristics of spherical vacuum voids *Astrophys. J.* **298** 439
[23] Khakshournia S and Mansouri R 2001 Formation of cosmological mass condensation within a FRW universe: exact general relativistic solutions *Phys. Rev.* D **65** 027302
[24] Anchordoqui L *et al* 2001 Brane worlds, string cosmology, and AdS/CFT *Phys. Rev.* D **64** 084027
[25] Vilenkin A 1984 Cosmic strings and domain walls *Phys. Rep.* **121** 263
[26] Blau S K, Guendelman E I and Guth A H 1987 Dynamics of false vacuum-bubbles *Phys. Rev.* D **36** 2919
[27] Berezin V A and Kuzmin V A 1987 Dynamics of bubbles in general relativity *Phys. Rev.* D **35** 1747
[28] Farhi E, Guth A H and Guven J 1990 Is it possible to create a universe in the laboratory by quantum tunneling? *Nucl. Phys.* B **339** 417
[29] Sakai N and Maeda K 1994 Junction conditions of Friedmann–Robertson–Walker space-times *Phys. Rev.* D **50** 5425
[30] Vick D 1986 Gravitational collapse of a shell subject to the Casimir force *Nouvo Cimento* B **94** 54
[31] Israel W 1966 Singular hypersurfaces and thin shells in general relativity *Nouvo Cimento* B **44** 1; 1967 *Nouvo Cimento* B **48** 463 (erratum)
[32] Núñez D, Oliveira H P and Salim J 1993 Dynamics and collision of massive shells in curved backgrounds *Class. Quantum Grav.* **10** 1117
[33] Goldwirth D S and Katz J 1995 A comment on junction and energy conditions in thin shells *Class. Quantum Grav.* **12** 769
[34] Fayos F, Senovilla J M M and Torres R 1996 General matching of two spherically symmetric spacetimes *Phys. Rev.* D **54** 4862
[35] Núñez D 1997 Oscillating shells: a model for a variable cosmic object *Astrophys. J.* **482** 963
[36] Nakao K, Ida D and Sugiura N 1999 Crossing of spherical massive shells in vacuum space-time *Prog. Theor. Phys.* **101** 1
[37] Gonçalves S M C V 2002 Relativistic shells: Dynamics, horizons, and shell crossing *Phys. Rev.* D **66** 084021
[38] Kirchner U 2004 A new approach to spherically symmetric junction surfaces and the matching of FLRW regions *Class. Quantum Grav.* **21** 3845
[39] Khorrami M and Mansouri R 1990 Spherically symmetric thin walls *Phys. Rev.* D **44** 557
[40] Mansouri R and Khorrami M 1996 The equivalence of Darmois–Israel- and distributional-method for thin shells in general relativity *J. Math. Phys.* **37** 5672
[41] Nozari K and Mansouri R 2002 The methods of gluing manifolds in general relativity *J. Math. Phys.* **43** 1519
[42] Hájíček P and Bičák J 1997 Gauge-invariant Hamiltonian formalism for spherically symmetric gravitating shells *Phys. Rev.* D **56** 4706
[43] Ansoldi A, Aurilia A, Balbinot R and Spalluci E 1997 Classical and quantum shell dynamics, and vacuum decay *Class. Quantum Grav.* **14** 2727
[44] Gladush V D 2001 On the variational principle for dust shells in General Relativity *J. Math. Phys.* **42** 2590
[45] Crisóstomo J and Olea R 2004 Hamiltonian Treatment of the Gravitational Collapse of Thin Shells *Phys. Rev.* D **69** 104023
[46] Kijowski J and Czuchry E 2005 Dynamics of a self-gravitating shell of matter *Phys. Rev.* D **72** 084015

[47] Hoye J S, Linerud I, Olaussen K and Sollie R 1985 Evolution of Spherical Shells in General Relativity it Physica Scripta **31** 97
[48] Khakshournia S and Mansouri R 2002 Dynamics of general relativistic spherically symmetric dust thick shells *Gen. Rel. Grav.* **34** 1847
[49] Fackerell E D 1975 The concentric shell method for relativistic star clusters *International Astronomical Union* Symposium no. 69, Dordrecht; Boston: D. Reidel Pub. Co., 433
[50] Eid A and Langer J 2000 On the crossing of thin shells *Czechoslovak J. Phys.* **50** 1081
[51] Langlois D, Maeda K and Wands D 2002 Conservation laws for collisions of branes and shells in general relativity *Phys. Rev. Lett.* **88** 181301
[52] The open source code of this C++ package, along with the pertinent executables, can be downloaded from `http://`**sss.rmki.kfki.hu**
[53] Wald R M: *General relativity*, University of Chicago Press, Chicago (1984)
[54] Barceló C and Visser M 2002 Twilight for the energy conditions? *Int. J. Mod. Phys.* D **11** 1
[55] Kijowski J, Magli G and Malafarina D 2006 Relativistic dynamics of spherical timelike shells *Gen Rel. Grav.* **38** 1697
[56] Gáspár M E *in preparation*
[57] Frauendiener J and Klein C 1995 On crossing dust shells *J. Math. Phys.* **36** 3632
[58] Krisch J P and Glass E N 2008 Thin shell dynamics and equations of state *Phys. Rev.* D **78** 044003
[59] Krisch J P and Glass E N 20087 Collapsing layers on Schwarzschild–Lemaitre geodesics *Phys. Rev.* D **76** 104006
[60] Read J S, Lackey B D, Owen B J and Friedman J L 2008 Constraints on a phenomenologically parametrized neutron-star equation of state *Phys. Rev.* D **79** 124032
[61] Visser M 1991 Quantum wormholes *Phys. Rev.* D **43** 402
[62] Dolgov A D and Khriplovich I B 1997 Properties of the quantized gravitating dust shell *Phys. Lett.* B **400** 12
[63] Szekeres P and Luna A 1999 What is a shell-crossing singularity? *J. Australian Math. Soc.* B. *Applied Mathematics* **41** 167
[64] Csizmadia P and Rácz I 2010 Gravitational collapse and topology change in spherically symmetric dynamical systems *Class. Quantum Grav.* **27** 015001